Research Square

Preprints are preliminary reports that have not undergone peer review.
They should not be considered conclusive, used to inform clinical practice,
or referenced by the media as validated information.

Mouse models of activity-based anorexia and binge-eating disorder show distinct patterns of intestinal barrier dysfunction and immune dysregulation

Petra Prochazkova

petra.prochazkova@mbu.cas.cz

Institute of Microbiology of the Czech Academy of Sciences

Helena Knotkova

Institute of Microbiology of the Czech Academy of Sciences

Janet Luthar

Institute of Microbiology of the Czech Academy of Sciences

Radka Roubalova

Institute of Microbiology of the Czech Academy of Sciences

Michal Kraus

Institute of Microbiology of the Czech Academy of Sciences

Toghrul Naghiyev

Institute of Microbiology of the Czech Academy of Sciences

Enrico Patrono

Institute of Microbiology of the Czech Academy of Sciences

Helena Tlaskalova-Hogenova

Institute of Microbiology of the Czech Academy of Sciences

Hana Papezova

Charles University and General University Hospital in Prague

Research Article

Keywords: gut permeability, tight junction, claudin, inflammation, ABA model, BED model, anorexia nervosa, binge-eating, microbiota-gut-brain axis

Posted Date: September 9th, 2026

DOI: https://doi.org/10.21203/rs.3.rs-10776674/v1

License: This work is licensed under a Creative Commons Attribution 4.0 International License.
Read Full License

Additional Declarations: No competing interests reported.

Abstract

Eating disorders involve interconnected metabolic, intestinal, and immune disturbances; however, how restrictive versus binge-eating behaviors differentially shape immune dysregulation remains unclear. Here, we compared barrier integrity and T cell–mediated immune responses in two mouse models of eating disorders: activity-based anorexia model (ABA), combining food restriction with voluntary wheel running, and binge-eating disorder model (BED), combining intermittent access to chocolate with food restriction stress or restraint stress.

Both models were robust. ABA mice (female Balb/c) showed rapid weight loss and hyperactivity, whereas BED mice (male C57Bl/6) persisted in chocolate-seeking despite aversive conditioning. Only ABA mice developed intestinal barrier dysfunction, with significantly increased FITC-dextran permeability during combined food restriction and exercise. Blood-brain barrier integrity remained intact in both models.

Gene expression profiling revealed distinct patterns of transcriptional Tight junction (TJ) remodeling. In ABA mice, colonic transcripts for *Tjp1, Cldn1, Cldn4, and Muc2* were reduced, consistent with an impaired epithelial barrier. BED mice showed broader disruption of junctional genes, characterized by decreased expression of sealing claudins and upregulation of *Cldn2*. *Cldn2* encodes a pore-forming claudin subtype whose increased expression is typically associated with enhanced paracellular cation permeability.

Immunologically, the two models produced opposite effects. ABA mice showed an immunosuppressive profile, with reduced T-cell proliferation in the spleen and mesenteric lymph nodes, lower IFN-γ and TGF-β production, and increased $CD4^{+}IL\text{-}10^{+}$ regulatory cells. BED mice showed a pro-inflammatory profile, with increased T-cell proliferation, elevated Th1/Th17 cytokine signatures, and a loss of $CD4^{+}TGF\text{-}\beta^{+}$ cells.

These findings suggest that restrictive and binge-eating phenotypes are associated with distinct alterations in intestinal barrier-related parameters and immune responses. Together, these results point to model-specific relationships between eating disorder-related phenotypes, intestinal barrier regulation, and immune alterations.

Background

Anorexia nervosa (AN) and binge-eating disorder (BED) represent two opposite extremes of dysregulated energy intake, yet both are associated with marked alterations in peripheral inflammation, gut microbiota composition, and neurocognitive function. Preclinical modeling of these conditions in rodents has primarily relied on the activity-based anorexia (ABA) paradigm for AN-like phenotypes (1) and the binge-eating diet model for hyperphagic behaviors (2–4).

Several variants of the ABA model have been developed to reproduce key features of AN, including food restriction, excessive physical activity, weight loss, and food-anticipatory activity. The classical ABA paradigm combines restricted food access with voluntary access to a running wheel, whereas modified

protocols vary the severity and duration of food restriction or include wheel-only and food-restricted control groups. These models allow the contribution of caloric restriction, physical activity, and their interaction to be investigated (5).

Similarly, a range of animal models have been developed to investigate specific behavioral and biological features of binge-eating disorder (BED), including intermittent or limited access to palatable food, cycles of food restriction and refeeding, and stress-induced binge-like eating (6, 7). These models reproduce different aspects of the disorder, such as excessive consumption of highly palatable food, stress-associated overeating, and compulsive-like food seeking.

The models also reveal systemic metabolic and inflammatory disturbances that parallel clinical findings. However, despite these shared physiological disruptions, it remains unclear how these paradigms differentially affect gut and brain barrier integrity and the downstream activation of peripheral immune pathways.

The integrity of barrier epithelia is essential for maintaining organismal homeostasis by preventing uncontrolled exchange between the internal and external environments. In the central nervous system, this function is conducted by the blood-brain barrier (BBB), a highly specialized endothelial interface whose tight junction (TJ) complexes limit paracellular permeability and regulate the trafficking of immune cells and solutes.

Analogously, the intestinal epithelium serves as the primary physical and immunological barrier separating the luminal microbiota and dietary antigens from the systemic circulation. TJ proteins, such as occludin, claudins, and junctional adhesion molecules (JAMs), are essential for maintaining barrier integrity and regulating paracellular permeability (8, 9). Dysregulation of these molecules has been linked to metabolic stress, systemic inflammation, and neurobehavioral alterations (10, 11). Recent evidence suggests that gut barrier and BBB function may be altered in eating disorders, potentially contributing to low-grade inflammation and dysregulated neural signaling (12).

Despite these insights, the impact of ABA- or BED-related stressors on gut and BBB permeability and on expression of TJ-associated genes remains poorly characterized. Functional assays using fluorescein isothiocyanate–dextran (FITC-dextran) enable *in vivo* assessment of barrier permeability, while gene expression analysis of TJ molecules provide mechanistic insight into barrier remodeling (13, 14).

In this study, we used mouse models of ABA and BED to investigate alterations in intestinal and BBB permeability, TJ-related gene expression, and associated immune responses. Rather than directly comparing two eating disorder models, we examined distinct stress paradigms associated with disordered eating: metabolic stress combined with hyperactivity in ABA versus intermittent caloric restriction and physical restraint in the BED paradigm. As caloric restriction may also engage homeostatic feeding pathways, the latter should be interpreted as a model of stress- and restriction-associated binge-like eating rather than a direct representation of clinical BED. We aimed to determine

whether these contrasting behavioral conditions converge on common pathophysiological alterations in gut and brain barrier integrity and subsequent peripheral and central immune responses.

Methods

Animal models of eating disorders

Approximately 6-week-old BALB/c (female) and C57BL/6 (male) mice were obtained from the breeding colonies of the Institute of Microbiology of the Czech Academy of Sciences. Mice were housed in individually ventilated cages in SPF conditions under controlled conditions with a 12 h light/12 h dark cycle at constant 22°C and fed a standard diet for mice and rats (Ssniff, Spezialdiäten GmbH, Germany). All procedures were conducted in accordance with EU legislation on the use of experimental animals (2010/63/EU) and the Czech Animal Welfare Act. Experimental protocols were approved by the Institute of Microbiology Animal Care and Use Committee (approval IDs: 12/2023 and 20–2022-P).

The ABA model requires a robust drive for wheel-running under food restriction; this response is markedly stronger in female BALB/c mice, a strain characterized by a heightened hypothalamic-pituitary-adrenal axis reactivity (15). Further, female mice were used because predominantly affects females, and sex-dependent hormonal mechanisms may contribute to susceptibility to ABA and estrogen-mediated modulation of orexigenic pathways. Female mice were used because AN predominantly affects females, and sex-dependent hormonal mechanisms may influence feeding behavior and susceptibility to ABA. Estrogen is an important regulator of hypothalamic energy balance and modulates orexigenic pathways, providing a biological rationale for investigating ABA in female mice (16).

In contrast, the BED phenotype in rodents is most faithfully reproduced in male C57Bl/6 mice, which exhibit rapid, high-fat diet-induced hyperphagia and display dopaminergic signaling changes that parallel human neuroimaging findings (17, 18). Pilot experiments in our laboratory showed that female C57Bl/6 mice do not develop a stable BED binge phenotype, while male BALB/c mice fail to engage in the wheel-running component of ABA. Including those groups would therefore add noise rather than informative contrast. Selecting these strain-sex combinations therefore maximizes phenotype fidelity, reduces the total number of animals needed to detect a biologically meaningful effect, and aligns with the 3-R principles of animal research. Moreover, generating four experimental groups (C57Bl/6 M/F, BALB/c M/F) would at least double the number of animals and exceed the approved animal-use protocol.

Animals were randomly assigned to experimental groups using a computer-generated randomization procedure. Data collection and sample processing were performed in a randomized order, with samples from different experimental groups distributed across processing batches to minimize potential batch effects. Investigators performing behavioral, permeability, gene expression, and immunological analyses were blinded to group allocation whenever feasible. Sample size was determined a priori by power analysis based on expected effect sizes from previous studies using ABA and BED models. The analysis

indicated that the selected sample size would provide at least 80% statistical power to detect biologically meaningful differences between groups at a significance level of $\alpha = 0.05$.

For establishment of the ABA model (Fig. 1), female BALB/c mice were randomly assigned to four groups: fed *ad libitum* (Ctrl) or food-restricted (FR) mice without running wheel access, and Ctrl or FR mice with access to a running wheel (W, FRW). Because ABA mice must be housed individually, experiments were performed four times using a total of 20 BALB/c mice per group.

Mice were acclimatized for 3 days with locked running wheels and food *ad libitum*. This was followed by a 7-day baseline phase during which running wheels (ENV-047, Med Associates, USA) were unlocked and body weight, food intake, and running activity were recorded. Baseline food intake was used to calculate the daily ration (g chow per g body weight). During the ABA phase, FR mice received 70% of their baseline food intake. After 7 days, mice were euthanized, and serum, brain, and gut tissues were collected. Mice were euthanized by cervical dislocation in accordance with institutional and national ethical guidelines.

The ABA experiment was performed four times. Because administration of fluorescein-labeled dextran interferes with subsequent gene-expression analyses, samples from different experimental runs were used for downstream assays. Flow-cytometric analyses were performed on samples obtained from two independent experimental replicates.

For the BED experiments, we used a mouse model combining repeated exposure to chocolate with food restriction (FR) or restraint stress (R) to capture both the motivational and stress-related components of binge-like eating. Highly palatable foods, particularly those rich in sugar and fat, are commonly consumed during binge-eating episodes, whereas food restriction and psychological stress are recognized triggers that can promote binge eating. By incorporating two distinct stressors, this model allowed us to examine whether different precipitating factors associated with binge-like eating induce distinct alterations in intestinal barrier function and immune responses. In addition, the conditioned suppression paradigm enabled us to assess persistent chocolate-seeking behavior despite an aversive association, providing a measure of compulsive-like food seeking.

For the BED mouse model (Fig. 2), experiments were performed three times using a total of 24 male C57BL/6 mice per group. Mice were exposed to either a food-related or a non-food-related chronic stressor to model binge-like behavior. To ensure comparable chronicity, both stressors were applied for 7 consecutive days. Mice were assigned to one of three groups: food restriction (FR), restraint (R), or non-stressed controls (Ctrl). FR mice were single-housed and subjected to mild chronic caloric restriction designed to induce a ~ 15% loss in body weight, with food provided once daily. After the restriction period, FR mice were returned to *ad libitum* feeding and regained baseline weight within 24 h; caloric restriction ended 13 days before behavioral testing to ensure satiety at test. R mice were group-housed and subjected to daily physical restraint (1 h/day) in ventilated tubes under dark, sound-attenuated conditions, with *ad libitum* access to food. Control mice remained undisturbed in their home cages.

To assess compulsive seeking and consumption of palatable food, all mice underwent a conditioned suppression paradigm (CSP) (days 12–19), using a validated model of compulsive-like behavior. Prior to CSP, mice were briefly exposed to chocolate (days 8–9) to minimize novelty effects, followed by 2 rest days (days 10–11). During CSP, mice were trained to associate a specific chamber with food or chocolate reward, followed by a light–footshock conditioning session. On test days, reward-seeking and consumption were assessed in the presence of the conditioned stimulus (light) in the absence of footshock. Behavioral measures included time spent in each chamber, number of entries, and reward consumption. Blood samples were collected 60 min after the test, and mice were sacrificed for downstream analyses (4).

In-vivo measurement of gut permeability

Intestinal permeability was assessed using oral gavage of fluorescein isothiocyanate (FITC–dextran 4 kDa; TdB labs, Sweden). Prior to the assay, mice were fasted for 3 h to allow gastric emptying. Baseline blood samples were collected from tail veins, after which mice were orally gavaged with FITC-dextran (10 mg in 100 µL sterile water). Besides administering a fixed amount of FITC-dextran, we also used a body weight–adjusted oral dose to assess whether the mouse body weight was associated with serum fluorescence levels (500 µg per 1 g body weight). Mice were kept fasted, and 3 h after gavage, blood samples were again collected from the tail vein for serum preparation.

As a preliminary step to determine the optimal time point for blood collection, serum was collected at 1, 2, 3, and 4 h following FITC-dextran gavage; 3 h was selected for all subsequent measurements. Serum samples were diluted with 15% acid citrate dextrose (Sigma-Aldrich, Germany) based on serum volume, centrifuged at 5,000 rpm for 10 min at 4°C, and the supernatant was kept on ice until fluorescence measurement.

For assessment of BBB permeability, brains were rapidly removed and rinsed in cold PBS to remove residual blood. Tissues were then transferred into 1 mL of PBS and homogenized using a FastPrep-24 homogenizer (MGP, Czech Republic) with Lysing Matrix D (MGP, Czech Republic). Homogenization was performed twice for 2 min at 5.5 m/s. Homogenates were centrifuged at 14,000 rpm for 20 min at 4°C, and the resulting supernatants were collected and used for permeability measurements. Brains from non-gavaged mice served as negative controls to confirm baseline signal and assay performance.

Indomethacin (Sigma Aldrich, Germany), used as a positive control for increased intestinal permeability, was dissolved in 100% dimethyl sulfoxide (Sigma Aldrich, Germany) and subsequently diluted in sodium bicarbonate buffer (Sigma Aldrich, Germany) prior to administration. Positive control received indomethacin at a final dose of 500 µg per mouse in 100 ul.

FITC-dextran concentrations were determined by interpolation from a standard curve generated using serial dilutions of FITC-dextran. Standards and samples were measured in duplicate. **Samples were diluted 2× in PBS before the measurement. Background fluorescence values of the plates were**

subtracted from all readings prior to analysis. Baseline serum fluorescence measured prior to gavage was subtracted from post-gavage fluorescence values for each mouse. **Fluorescence measurements were performed in black 96-well plates using a spectrophotometer (Infinity M Plex, Tecan, Switzerland) with excitation at 485 nm and emission at 530 nm.** All measurements were performed in a light-protected environment.

Analyses of the expression of TJ molecules

Baseline expression of genes associated with intestinal and BBB permeability was assessed in colon and hypothalamus tissues from naïve BALB/c mice (n = 6). Tissues were rapidly dissected, and total RNA was isolated using TRIzol reagent (Thermo Fisher Scientific, USA) according to the manufacturer's instructions. RNA (1 µg), treated with TURBO DNase I (Thermo Fisher Scientific, USA), was reverse-transcribed using oligo$(dT)_{12\text{-}18}$ primers and SuperScript IV reverse transcriptase (Life Technologies, USA). Non–reverse transcription controls were included to exclude genomic DNA contamination.

Quantitative real-time PCR was performed on generated cDNA using a CFX96 Touch™ system (Bio-Rad, USA) with gene-specific primers (Table S1). Amplification efficiency was verified using a cDNA dilution series. Cycling conditions were 4 min at 94°C, followed by 35 cycles of 10 s at 94°C and 25 s at 60°C, with a final extension at 72°C for 7 min. Primer specificity was confirmed by melt curve analysis. Gene expression was calculated using the $2^{-\Delta\Delta CT}$ (Livak) method and normalized to the two most stable reference genes (ACTB and GAPDH), identified using RefFinder (Fig. S1). All reactions were run in duplicate, and non-template controls were included. Data are presented as mean ± SD.

Measurement of serum inflammatory and intestinal barrier function markers

Immediately following euthanasia, whole blood was collected by cardiac puncture into Micro Sample Tubes Serum Gel CAT (1.1 mL; Sarstedt, Germany). Samples were allowed to clot at room temperature for 20–30 min, then centrifuged at 2,000 × g for 10 min at 4°C. The resulting serum was collected, aliquoted, and stored at − 80°C until analysis. Serum concentrations of sCD14 (secretory CD14), calprotectin, serum amyloid A (SAA), and lipopolysaccharide-binding protein (LBP) were quantified using commercially available ELISA kits (Duo-Set ELISA Kits; R&D Systems, USA), according to the manufacturer's instructions.

Analyses were performed in duplicate, with serum diluted 500-fold for LBP analysis and 2-fold for sCD14, calprotectin, and serum amyloid A. For all analyses, absorbances at 450 nm with reference correction at 650 nm were measured using a Multiskan Ascent Plate Reader Spectrometer (MTX Lab Systems, USA).

Flow cytometry analysis

Spleens and mesenteric lymph nodes (MLN) were collected immediately after sacrifice and processed under sterile conditions. Spleens were mechanically dissociated through a 70-µm cell strainer to obtain single-cell suspensions. Red blood cells were lysed using ammonium-chloride-potassium lysis buffer (ACK; Ardeapharma, Czech Republic), followed by washing in cold phosphate-buffered saline (PBS; Ardeapharma, Czech Republic). MLN were mechanically disrupted through a 70-µm cell strainer (Avantor, Czech Republic) in cold PBS. Cell suspensions from both tissues were washed and resuspended in complete RPMI (Merck, Germany), containing 10% heat-inactivated fetal bovine serum and antibiotic-antimycotic solution (Sigma-Aldrich, Germany). Cell counts and viability were determined using trypan blue exclusion.

For surface marker (CD3, CD4, CD8, CD25) as well as for intracellular transcription factor analyses (FoxP3, T-bet, GATA3, Ki-67), $1–2 \times 10^5$ cells were labeled with Fixable Viability Dye (Thermo Fisher Scientific, USA), fixed, and permeabilized with eBioscience™ FoxP3/Transcription Factor Staining Buffer Sets (Thermo Fisher Scientific, USA). Non-specific staining was blocked with 10% normal mouse serum and Fc-receptor blocking reagent (anti-CD16/CD32 antibody); cells were stained for T-cell markers using fluorescence-labeled antibodies (Table S2). For cytokine detection (IFN-γ, IL-17A, IL-10, TGF-β), splenocytes and MLN cells were stimulated *ex vivo* with plate-bound 5 µg/mL anti-CD3ε and 4 µg/mL of anti-CD28 (Table S2) for 18 h at 37°C in 5% CO_2. For the last 4 h of incubation, a mixture of 3 µg/mL of Brefeldin A and 2 µM Monensin (Thermo Fisher Scientific, USA) was added.

Following stimulation, cells were washed, labeled with Fixable Viability Dye (Thermo Fisher Scientific, USA), fixed and permeabilized with a eBioscience™ Intracellular Fixation & Permeabilization Buffer Set (Thermo Fisher Scientific, USA), blocked with Fc-receptor blocking reagent, and stained for CD3, CD4, CD8, IFN-γ, IL-17A, IL-10, and TGF-β (Table S2). Data were acquired on a ZE5 multicolor flow cytometer (Bio-Rad, USA). Compensation was performed using single-stained controls and compensation beads (Thermo Fisher Scientific, USA), and fluorescence-minus-one (FMO) controls were used to define gating boundaries. A minimum of 50,000–100,000 lymphocyte-gated events were collected per sample. Gating strategies are shown in Figs. S2–3. Results are expressed as the percentage of positive cells within the $CD3^+$, $CD4^+$, or $CD8^+$ T-cell compartment.

Statistical analysis

Serum and brain levels of translocated FITC-dextran were analyzed via one-way ANOVA and Tukey's post hoc test. Data from RT-qPCR as well as serum biomarkers reflecting inflammation and endotoxin exposure were analyzed via one-way ANOVA using Box–Cox-transformed values ($\lambda = 0.1$) and Tukey's post hoc test. For datasets that did not meet the assumptions of parametric analysis, a Box–Cox transformation was applied before performing ANOVA. Correlations between variables were explored using Spearman's rank correlation. Flow cytometry data were analyzed via one-way ANOVA and Tukey's post hoc test. Immunohistology signals were analyzed using the non-parametric Kruskal–Wallis test. Statistical significance was defined as: $p < 0.05$ (*), $p < 0.01$ (**), $p < 0.001$ (***), and $p < 0.0001$ (****). All analyses were performed using GraphPad Prism 8 and RStudio (v2023.6.0.421).

Results

Study design

We employed two complementary rodent models to investigate distinct eating-disorder phenotypes. The BED model was performed in male C57Bl/6 mice because this strain readily exhibits binge-type hyperphagia on a high-fat diet and is the most widely used background for operant-reward testing. The ABA model was conducted in female BALB/c mice, a sex-strain combination that reliably shows excessive running wheel activity combined with weight loss under food restriction. Consequently, each model was run in the strain/sex that maximises translational relevance for the specific disorder, but this also introduces strain- and sex-dependent variables that must be considered when interpreting cross-model comparisons.

Establishment and verification of the ABA and BED experimental models

During experiments with the ABA model, the body weight of all mice was recorded, and the running wheel activity of mice, in groups with wheel access, was monitored. Although mice in the food-restricted group without wheel access showed a significant weight reduction compared to controls, weight loss in the ABA group was even more pronounced. Furthermore, mice exposed to caloric restriction in the ABA paradigm spontaneously increased their physical activity compared to mice fed *ad libitum* (Fig. 3A–B).

In the BED mouse model, during the testing phase of the experiment, the time each mouse spent in each compartment of the apparatus was recorded. Across experimental groups, the figure presents the mean time each mouse spent in the three compartments of the apparatus (chocolate room, alley, and no-chocolate room). Mice previously exposed to food-restriction stress or restraint stress spent significantly more time in the room with chocolate than in the room without chocolate, despite prior conditioning to associate this compartment with footshock. Mice exposed to restraint stress also spent significantly more time in the room with chocolate than non-stressed controls (Fig. 3C). Additionally, food-restricted mice consumed a significantly greater amount of chocolate than both control and restraint-stressed mice (Fig. 3D). Overall, these results confirm the successful establishment of the BED model for further measurements.

Increased intestinal but not BBB permeability in ABA mice

To quantify intestinal permeability in the both models, we performed FITC-dextran gavage followed by serum and brain homogenate fluorescence measurement. Time-course analysis following oral gavage of FITC-dextran (4 kDa) revealed that serum fluorescence peaked at 3 hours post-gavage in both BALB/c and C57BL/6 mice, indicating this as the optimal time point for blood sampling (Fig. 4A–B). Oral administration of indomethacin, used as a positive control due to its recognized ability to increase intestinal permeability, resulted in a marked increase in serum FITC-dextran fluorescence, confirming the sensitivity of the assay (Fig. 4C–D).

Assessment of barrier permeability using FITC-dextran revealed a significant increase in intestinal permeability in the ABA model, specifically in the food-restriction with wheel-access (FRW) group, as indicated by elevated serum FITC-dextran levels. No significant differences in intestinal permeability were observed in the FR, or W groups (Fig. 5A). In the BED model, no differences in intestinal permeability were detected among the Ctrl, FR, and R groups (Fig. 5B). To exclude the possibility that differences in body weight influenced FITC-dextran translocation, a Spearman correlation analysis was performed, which showed no significant association between body weight and serum FITC-dextran levels when FITC-dextran was administered as either a fixed absolute dose (Fig. 5E–F) or a dose adjusted to body weight (Fig. S4).

We also evaluated BBB integrity by orally administering 4-kDa FITC-dextran. After a single gavage, fluorescence was measured in brain tissue to determine whether the tracer crossed the BBB from the systemic circulation. Indomethacin treatment markedly increased FITC-dextran fluorescence in brain homogenates compared to vehicle-treated controls, indicating enhanced BBB permeability. Peak accumulation occurred 2–3 hours after dextran administration, when fluorescence levels were significantly higher than in mice that did not receive indomethacin. This temporal profile indicates that indomethacin transiently enhances BBB permeability, with maximal tracer penetration during the 2–3 hour post-dose window (Fig. S5). In contrast, FITC-dextran levels in the brain tissue of ABA and BED mice were indistinguishable from their respective controls, and values overlapped with those of mice not administered FITC-dextran. These findings indicate that any BBB alterations in these models are either below the detection threshold of this assay method, which call ask the sensitivity required to detect microvascular changes in permeability, or involve mechanisms not captured by bulk tracer permeability (Fig. S5).

Differential regulation of intestinal and hypothalamic barrier-related genes in ABA and BED models

RefFinder (19) was used to assess the stability of six candidate housekeeping genes (*Gapdh, Actb, Hprt, Pgk1, S12, Casc3*). The combination of Actb and Gapdh was identified as the most stable reference set for both tissues (Fig. S1). Amplification efficiencies for all target genes ranged from 92.3% to 109.8%.

Analysis of barrier-associated gene expression revealed markedly tissue-specific profiles. In the colon, the highest transcript levels were observed for TJ genes *Tjp1*, *Tjp2*, and *Tjp3*, as well as *Muc2* and claudin genes *Cldn2*, *Cldn3*, *Cldn7*, and *Cldn12*, while *Cldn5*, *Cldn9*, and *Cldn19* were not detectable. In contrast, in the hypothalamus, the highest transcript levels were detected for *Cldn5, Cldn9, Cldn10, and Cldn19*, whereas *Tjp3*, *Muc2*, and *Cldn3 and Cldn4* were not detectable (Table 1).

In the colons of ABA-model mice, *Ocln* and *JAMA* transcript levels were increased in both the W and FRW groups compared with controls. *Cldn8* expression was elevated in all experimental groups. In contrast, *Muc2, Tjp1, and Cldn1* expression was decreased in the FRW group, while *Cldn4* expression was decreased in both the FR and FRW groups. Transcript levels of the remaining barrier-associated genes remained unchanged across experimental conditions (Fig. 6).

Analysis of colonic gene expression in BED mice revealed distinct alterations in TJ and permeability-associated genes in FR and R mice compared with controls. The core sealing genes *Ocln*, *JAM-A*, and *Cldn1* were downregulated in both FR and R groups, suggesting reduced TJ sealing capacity irrespective of the post-binge feeding regimen. In contrast, the pore-forming, leak-promoting gene *Cldn2* was strongly upregulated in both FR and R groups, which may be associated with enhanced paracellular permeability. The barrier-strengthening claudin genes *Cldn3* and *Cldn7*, which are normally highly expressed in colonic epithelium, were significantly reduced only in the FR cohort. This suggests that the intermittent feeding restriction imposed an additional layer of barrier vulnerability beyond that caused by binge exposure alone. In the restraint-stress cohort, the sealing claudin gene *Cldn4* was uniquely decreased, whereas the non-canonical claudin gene *Cldn12*, which can enhance nutrient-linked ion transport, was markedly increased, hinting at stress-induced transcriptional remodeling of the junctional complex that may favor absorptive over barrier functions (Fig. 7).

To assess whether transcriptional changes in TJ genes were reflected at the protein level, colonic sections from ABA and BED mice were immunohistochemically stained for Claudin-1 and TJP-1. Both proteins displayed the expected epithelial localization; however, quantitative analysis revealed no significant differences in Claudin-1 or TJP-1 immunoreactivity between experimental and control groups in either model (Figs. S6–S9).

In the hypothalamus of ABA mice, *Ocln* mRNA expression was increased in both groups with access to running wheels compared with controls. *Tjp2* expression was elevated in all experimental groups compared to controls. In contrast, *Cldn5* expression was reduced in all three experimental groups relative to controls (Fig. 8A). In the hypothalamus of BED mice, gene-expression analysis revealed a slight increase in *JAMA* expression in the R group, while no other significant changes were detected among the experimental groups (Fig. 8B).

Serum markers of inflammation and gut barrier dysfunction in ABA and BED mice

To assess systemic inflammation and intestinal barrier function, serum inflammatory and intestinal barrier–associated markers were measured in both ABA and BED mouse models. ABA mice showed elevated serum concentrations of sCD14 and calprotectin, along with reduced levels of serum amyloid A and lipopolysaccharide-binding protein (LBP) compared to controls. These changes were also significant when comparing food-restricted mice with FRW mice. Relative to activity controls (W), FRW mice showed further suppression of circulating LBP and SAA (Fig. 9).

Assessment of these markers in the BED model revealed a significant decrease in SAA in both FR and R mice relative to controls. Although sCD14 and calprotectin showed a trend toward increased levels, these changes did not reach statistical significance. No differences in serum LBP concentrations were observed among groups (Fig. 9). Across all samples, **s**erum sCD14 concentrations were positively correlated with calprotectin concentrations, as determined by Spearman's rank correlation, in both ABA and BED models (Fig. 9).

ABA-induced suppression of T cell proliferation in systemic and mesenteric lymph nodes

To evaluate the effects of food restriction and voluntary physical activity on T-cell homeostasis, proliferative and functional $CD4^+$ and $CD8^+$ T-cell subsets were analyzed in the spleen and mesenteric lymph nodes (MLN) of mice subjected to the ABA protocol.

In the spleen, food restriction was associated with reduced proliferative activity of $CD4^+$ T cells, as significantly decreased frequencies of $CD4^+Ki\text{-}67^+$ cells were observed in both FR and FRW mice. Proliferation of $CD8^+$ T cells and $CD4^+CD25^+FoxP3^+$ regulatory T cells was reduced in all experimental groups. In contrast, decreased proliferation of $CD4^+T\text{-}bet^+$ and $CD4^+GATA3^+$ cells was observed exclusively in the FRW group, which also showed a reduced frequency of total $CD4^+GATA3^+$ cells. These findings indicate that while food restriction and wheel access independently affected the proliferative activity of selected splenic T-cell populations, their combination exerted a broader suppressive effect on Th1- and Th2-associated $CD4^+$ T-cell subsets (Fig. 10).

In the MLN, both groups with access to running wheels (W and FRW) showed significantly reduced frequencies of proliferating T cells, including $CD4^+Ki\text{-}67^+$ and $CD8^+Ki\text{-}67^+$ subsets, compared with control mice, indicating that voluntary exercise markedly impairs T-cell proliferative activity within gut-associated lymphoid tissue (GALT). Additionally, proliferating regulatory T cells ($CD4^+CD25^+FoxP3^+Ki\text{-}67^+$; Tregs) and total $CD4^+GATA3^+$ cells (Th2 phenotype) were significantly decreased in both W and FRW groups relative to controls, suggesting attenuated Th2-associated immune responses in the intestinal compartment. A selective reduction in proliferating $CD4^+T\text{-}bet^+Ki\text{-}67^+$ cells (Th1 phenotype) was observed only in the FRW group, indicating that the combination of caloric restriction and physical activity exerts a particularly strong suppressive effect on proliferating Th1 cells in the MLN (Fig. 10).

Collectively, these findings demonstrate that the ABA model, particularly the combination of caloric restriction and excessive physical activity in the FRW group, induces profound suppression of T-cell proliferation and reshapes helper T-cell subset composition in both systemic (spleen) and gut-associated (MLN) immune compartments. These effects were most pronounced in proliferating Th1, Th2, and regulatory T-cell populations.

Enhanced T-cell proliferation and Th1-associated responses in the BED model

To evaluate the effects of food restriction and restraint stress on intestinal immune homeostasis in the BED model, T-cell populations and their proliferative activity were analyzed in the spleen and MLN.

In the spleen, FR and R mice similarly displayed increased proliferation of $CD4^+$ T cells, while enhanced $CD8^+$ T-cell proliferation was observed specifically in the R group. Although $CD4^+$ T-cell frequencies were reduced, $CD8^+$ T-cell proportions were increased in both groups, indicating a shift in systemic T-cell composition toward the cytotoxic compartment under food restriction and restraint stress. Analysis of

regulatory T cells in the spleen revealed increased frequencies of proliferating Tregs in the FR group, accompanied by an elevated total percentage of Tregs, suggesting enhanced expansion of immunoregulatory subsets in response to food restriction stress. In addition, both FR and R mice showed significantly increased frequencies of $CD4^+$T-bet^+ cells and proliferating $CD4^+$T-$bet^+$$Ki\text{-}67^+$ cells, indicating activation and expansion of Th1-associated immune responses in the spleen. In contrast, the proportion of $CD4^+GATA3^+$ cells increased only in the FR group, while proliferative activity in this subset remained unchanged, suggesting selective modulation of Th2-associated cell abundance without altered proliferative dynamics (Fig. 11).

In the MLN, both food-restricted (FR) and restraint-stressed (R) mice showed higher frequencies of proliferating $CD4^+Ki\text{-}67^+$ and $CD8^+Ki\text{-}67^+$ T cells than controls, indicating enhanced T-cell activation within GALT. Proliferating regulatory T cells ($CD4^+CD25^+FoxP3^+Ki\text{-}67^+$) were also elevated in both groups. Despite this increase in proliferative activity, the overall proportion of $CD4^+$ T cells was slightly reduced, whereas Treg frequencies were elevated in FR mice, suggesting a shift toward a more regulatory T-cell phenotype, driven by increased Treg proliferation and elevated Treg frequencies under food-restriction conditions (Fig. 11). Both FR and R groups showed increased frequencies and proliferation of $CD4^+$T-bet^+ cells, consistent with enhanced Th1-associated responses. In contrast, $CD4^+GATA3^+$ cell frequencies and proliferation remained unchanged (Fig. 11).

Collectively, these findings demonstrate that food restriction and restraint stress induce substantial alterations in T-cell homeostasis in both gut-associated and systemic immune compartments, characterized by enhanced proliferative activity, expansion of Th1-associated subsets, and altered frequencies of regulatory and cytotoxic T-cell populations.

The ABA model induces distinct changes in $CD4^+$ and $CD8^+$ T cell cytokine profiles

To evaluate the effects of the ABA paradigm on T-cell effector function, cytokine production by $CD4^+$ and $CD8^+$ T cells was analyzed in MLN and spleen. Similar cytokine patterns were observed in both immune compartments.

In both the MLN and spleen, the FRW group showed significantly reduced frequencies of IFN-γ–producing $CD4^+$ T cells compared with controls. Similarly, frequencies of $CD8^+$IFN-γ^+ T cells were decreased in both FR and FRW groups, indicating impaired cytotoxic and Th1-associated effector responses under caloric restriction, especially when combined with hyperactivity (Fig. 12).

Analysis of TGF-β–producing T cells revealed tissue-specific alterations. In the MLN, frequencies of both $CD4^+$TGF-β^+ and $CD8^+$TGF-β^+ cells were significantly reduced across all experimental groups compared with controls. In the spleen, however, decreased frequencies of TGF-β–producing $CD4^+$ and $CD8^+$ T cells were observed only in the FRW group, suggesting a generalized suppression of TGF-β–mediated regulatory pathways in the gut-associated lymphoid tissue (Fig. 12).

The FRW group also exhibited a significant increase in $CD4^+IL\text{-}10^+$ T cells in both tissues, indicating a compensatory upregulation of IL-10–producing T cells under combined metabolic and physical stress. No significant differences were observed in $CD8^+IL\text{-}10^+$ cell frequencies among experimental groups (Fig. 12).

A significant decrease in the frequency of $CD4^+IL\text{-}17A^+$ T cells in both FR and FRW groups, restricted to the spleen and absent in the MLN, indicates that attenuation of the Th17-associated response is systemic rather than intestinal. This finding suggests that caloric restriction negatively impacts splenic Th17 populations, independent of exercise.

Collectively, these results demonstrate that the ABA model induces marked alterations in T-cell cytokine production in both gut-associated and systemic immune compartments, characterized by suppression of IFN-γ responses, enhanced IL-10 production by $CD4^+$ T cells, and reduced TGF-β expression, particularly under combined food restriction and hyperactivity.

Food restriction and restraint stress proinflammatory T cell cytokine responses in the BED model

To determine the impact of binge-eating–related conditions on T-cell effector function, intracellular cytokine production was analyzed in $CD4^+$ and $CD8^+$ T cells isolated from the MLN and spleen. Overall, food restriction and restraint stress induced a predominantly pro-inflammatory cytokine profile across both immune compartments.

Increased frequencies of $CD4^+IL\text{-}17A^+$ T cells were observed in the FR group in both MLN and spleen, whereas elevated frequencies in the R group were restricted to the spleen. These findings indicate enhanced Th17-associated responses, particularly under food-restriction conditions (Fig. 13).

In the spleen, both FR and R mice exhibited increased frequencies of $CD4^+IFN\text{-}\gamma^+$ T cells compared with controls, suggesting enhanced systemic Th1-associated activity. Similarly, frequencies of $CD8^+IFN\text{-}\gamma^+$ T cells were increased specifically in the R group, indicating enhanced cytotoxic effector activity in response to restraint stress. In contrast, IFN-γ production remained unchanged in the MLN across all groups (Fig. 13).

No significant changes were detected in the frequencies of $CD4^+IL\text{-}10^+$ T cells among experimental groups in either tissue. However, frequencies of $CD8^+IL\text{-}10^+$ T cells were increased in both FR and R groups in the MLN and spleen, although the overall frequency of these cells remained relatively low (Fig. 13).

Analysis of TGF-β production demonstrated significantly reduced frequencies of $CD4^+TGF\text{-}\beta^+$ cells in both FR and R groups in the MLN and spleen, indicating impaired regulatory T-cell–associated cytokine responses under both food-restriction and restraint-stress conditions. In contrast, frequencies of $CD8^+TGF\text{-}\beta^+$ cells remained unchanged across experimental groups (Fig. 13).

Collectively, these findings demonstrate that food restriction and restraint stress in the BED model promote predominantly pro-inflammatory T-cell responses, characterized by enhanced Th1- and Th17-associated cytokine responses together with reduced frequencies of $CD4^+TGF\text{-}\beta^+$ regulatory T cells, while IL-10–producing T-cell frequencies remain largely unchanged except for a modest increase in $CD8^+IL\text{-}10^+$ cells.

Discussion

In this study, we examined intestinal barrier integrity and T-cell–mediated immune responses in mouse models of anorexia nervosa (activity-based anorexia; ABA) and binge-eating disorder (BED). The ABA model was associated with increased intestinal permeability, reduced expression of TJ proteins, and an immunosuppressive phenotype, while the BED model exhibited TJ dysregulation and heightened pro-inflammatory immune responses. Importantly, these transcriptional changes in the BED model did not correspond to increased FITC-dextran permeability, indicating that BED induces transcriptional remodeling of junctional complexes without overt functional barrier breakdown. These findings indicate that restrictive behavior in female BALB/c mice and binge-eating behavior in male C57Bl/6 mice can induce distinct gut–immune alterations.

The ABA model mimics key features of AN by combining food restriction with hyperactivity–behaviors commonly observed in patients (20). The BED model is based on stress exposure being a contributing factor in the development of compulsive eating behavior (Latagliata et al. 2010, Brown and James 2023). In our study, we employed food-related (food restriction) and non-food-related stress (restraint), enabling us to disentangle how different stress modalities influence immune function and barrier regulation.

Using FITC-dextran assays, we demonstrated increased intestinal permeability specifically in the ABA model, while no significant barrier impairment was observed in the BED model (Fig. 5). We found that disruption of the intestinal barrier increased intestinal permeability, which may increase exposure to luminal antigens or microbial products and could subsequently contribute to systemic immune activation.

A commonly used method to assess intestinal paracellular permeability is the FITC-dextran assay, which measures the translocation of fluorescent dextran from the intestinal lumen into the bloodstream following oral administration. FITC-dextran (4 kDa) crosses the intestinal barrier only in lesser amounts under physiological conditions, allowing detection of modest increases in paracellular permeability when the barrier is compromised (21, 22).

In our study, we observed increased intestinal permeability in “anorexia nervosa-like” mice subjected to food restriction combined with running-wheel activity (FRW group), consistent with previous reports showing increased colonic permeability in ABA models with progressively restricted food access (23). Since this effect was not observed in the other experimental groups (i.e., controls for food restriction

alone (FR) or running-wheel access alone (W)), our findings suggest a crucial role for the combined effects of food restriction and physical activity in driving the observed increase in intestinal permeability.

Although some studies recommend adjusting FITC-dextran dosing according to body weight (24), our preliminary experiments in healthy mice using both a fixed and weight-adjusted doses revealed no correlation between body weight and serum FITC-dextran levels (Fig. 5, S4). Moreover, adjusting the dose based on body weight is challenging in our experimental setting due to only minor inter-individual differences in body weight between mice. Altered intestinal permeability in BED mice has not been extensively described to date. In our study, we did not observe significant changes in intestinal permeability in the BED mice, which may be attributable to the relatively short duration of the applied stress paradigm (Fig. 5).

Intravenous administration of FITC-dextran is generally preferred for assessing BBB permeability (25). However, in this study, we also examined whether brain levels of FITC-dextran could serve as a secondary measure of systemic distribution following oral administration used for gut permeability assessment. No significant differences in brain FITC-dextran levels were observed between experimental groups in either model. In contrast, indomethacin treatment resulted in higher brain FITC-dextran levels compared with untreated controls, suggesting increased BBB permeability under conditions of pharmacologically induced barrier disruption (Fig. S5).

Both intestinal and BBB permeability are closely regulated by the abundance and distribution of TJ proteins, which control paracellular transport across the intestinal epithelium. Reduced expression or altered localization of these molecules can impair barrier integrity and increase intestinal permeability (21). Although our measurements reflect mRNA expression, these transcriptional changes did not consistently translate into detectable protein-level differences, indicating post-transcriptional regulation or delayed protein turnover that may decouple transcript abundance from functional barrier outcomes. The intestinal epithelium and brain microvascular endothelium both contain overlapping but distinct sets of sealing proteins, and their tissue-specific expression patterns reflect their diverse barrier functions (26–28).

In colonic tissue, we detected the highest mRNA expression levels of *Tjp1*, *Tjp2*, *Tjp3*, *Muc2*, and the claudin genes *Cldn2*, *Cldn3*, *Cldn7*, and *Cldn12*, whereas in the hypothalamus, we observed the highest expression of *Cldn5*, *Cldn9*, *Cldn10*, and *Cldn19*. In accordance with endothelial single-cell atlases from the Carmeliet group (29), *JAMA*, *Tjp1*, and *Tjp2* were expressed in both tissues, although their cellular sources differ between colonic epithelium and brain endothelium (Table 1).

However, while their study detected low levels of *Cldn5* expression in the colon, this transcript was not detectable in our samples. Conversely, although *Ocln* expression was not observed in their dataset, we detected low levels of *Ocln* mRNA in the colon of our mice (29). These discrepancies may reflect methodological differences, as single-cell transcriptomic analyses and bulk RT-qPCR measurements differ in their sensitivity to low-abundance transcripts. Previous studies have shown very low transcript levels of *Cldn5* and *Cldn9* in colonic epithelial cells (30). Moreover, our analysis was limited to the

hypothalamus rather than the whole brain, as the hypothalamus plays a central role in the regulation of feeding behavior and food-seeking responses, which may further contribute to the observed differences in expression patterns.

In the colons of ABA-model mice, we observed increased mRNA expression of *Ocln*, *JAMA*, and *Cldn8*, and decreased expression of *Muc2*, *Tjp1*, *Cldn1*, and *Cldn4* in the FRW group (Fig. 6), indicating substantial transcriptional remodeling of the intestinal barrier. Increased *Ocln* expression in the FRW group was also reported in our previous study (31). The reduced expression of *Muc2*, *Tjp1*, *Cldn1*, and *Cldn4* suggests weakened epithelial barrier integrity and diminished mucosal protection, consistent with the increased intestinal permeability observed in this group (Fig. 6).

Since the proteins encoded by *Tjp1* and the *Cldn* genes are essential components of TJ complexes, reduced mRNA expression of these genes may limit the availability of their corresponding TJ proteins and thereby facilitate enhanced paracellular transport across the intestinal epithelium. Decreased *Muc2* expression may further compromise the protective mucus layer, increasing epithelial exposure to luminal antigens and microorganisms. Our findings agree with the study by Jesus et al. (23), who reported decreased colonic *Cldn1* expression in ABA mice compared with mice subjected to limited food access alone, further supporting the idea that the combination of food restriction and hyperactivity contributes to barrier impairment (23).

Increased expression of *Ocln and JAM-A* in the wheel-access groups may represent a compensatory response to preserve barrier integrity under increased activity. Similarly, elevated *Cldn8* expression across all experimental groups could reflect adaptive tightening of the epithelial barrier, since *Cldn8* is generally associated with barrier-sealing properties (32) (Fig. 6). The observed changes in TJ–related gene expression suggest complex transcriptional remodeling of the intestinal barrier in the ABA model.

Although we did not observe increased intestinal permeability in the BED model mice (Fig. 7), we detected significant changes in the colonic mRNA expression of several TJ–related genes. Specifically, decreased expression of *Ocln, JAM-A, and Cldn1*, along with increased expression of the pore-forming *Cldn2*, the gene encoding a pore-forming claudin subtype, suggests early disruption of epithelial barrier organization and a shift toward a more permeable intestinal phenotype. However, these transcriptional changes were likely either insufficient to induce overt barrier dysfunction or may represent an early stage of barrier impairment that precedes measurable increases in intestinal permeability. To our knowledge, studies investigating intestinal barrier integrity and TJ alterations in experimental models of BED are currently lacking, making direct comparison of our findings difficult. The absence of detectable permeability changes in our BED model may also be related to the relatively short duration of the applied stress and feeding protocol, which may not have been sufficient to elicit measurable functional impairment despite clear transcriptional changes in TJ–related genes.

An important consideration is that the increased intestinal permeability observed in the ABA model may not fully correspond to changes in colonic TJ protein expression. Because our measurements reflect mRNA levels, transcriptional alterations do not necessarily translate directly into proportional changes in

protein abundance or localization, both of which are critical determinants of barrier function. Thus, differences in post-transcriptional regulation, protein turnover, or junctional assembly may further contribute to the divergent permeability outcomes observed between the ABA and BED models.

Intestinal permeability assessed by FITC-dextran reflects the functional integrity of the gastrointestinal barrier across multiple intestinal segments, whereas our analyses of TJ–related mRNA and proteins were performed exclusively in the colon. Therefore, functional barrier alterations may originate from regions other than the colon or arise from mechanisms not directly captured by measurements of TJ transcript abundance. Moreover, barrier dysfunction can arise through post-transcriptional regulation, altered protein localization, or changes in mucus layer composition without producing proportional changes in gene expression. In addition, we recently demonstrated that the gut microbiota of FR and R mice differs significantly (33). Given the well-established role of the microbiota in regulating epithelial barrier function and transcription of TJ–related genes, these microbial differences may contribute to the distinct patterns of TJ gene expression observed between groups.

In the hypothalamus of the FRW group of ABA mice, we observed increased mRNA expression of *Ocln and Tjp2*, along with reduced expression of *Cldn5* compared with controls (Fig. 8). TJP-2, the protein encoded by *Tjp2*, is a scaffolding protein that links transmembrane TJ proteins to the cytoskeleton, and its upregulation may represent a compensatory or stabilizing response to metabolic challenges, potentially counterbalancing the reduced availability of Claudin-5 (which would be expected given the decreased *Cldn5* transcript levels). Claudin-5 is the major TJ adhesion protein in brain endothelial cells (Morita et al. 1999). This interpretation is supported by a previous study showing that loss of Claudin-5 leads to size-selective loosening of BBB TJ in endothelial cells (34). Although we did not detect increased BBB permeability using orally administered FITC-dextran, reduced *Cldn5* expression may still indicate subtle molecular changes in the BBB that precede overt functional barrier disruption.

The altered serum levels of inflammatory markers (sCD14 and calprotectin) and gut barrier–relevant microbial products (such as bacterial lipopolysaccharides) observed in FRW mice further support the presence of systemic consequences linked to intestinal barrier disruption in the ABA model. Increased circulating levels of sCD14 and calprotectin may indicate enhanced immune activation and greater exposure to microbial products originating from the intestinal lumen (Fig. 9). Secretory CD14 is commonly associated with host responses to bacterial lipopolysaccharides and microbial translocation (35), whereas calprotectin is linked to inflammatory activation and neutrophil-related immune responses (36). Similar results were reported in our previous study, although in germ-free mice (31). In contrast, decreased serum levels of SAA and LBP (Fig. 9) suggest that the inflammatory response in ABA mice may not correspond to a classical acute-phase reaction (37, 38). This pattern may reflect altered hepatic acute-phase protein production due to severe metabolic stress and malnutrition associated with the ABA condition.

The comparative analysis of the ABA and BED models revealed fundamentally distinct patterns of immune regulation in both gut-associated and systemic lymphoid tissues. The anorexia-like phenotype

was characterized primarily by suppression of T-cell proliferation and reduced effector cytokine production, whereas the stressors used in the BED model induced a markedly pro-inflammatory immune profile with increased T-cell activation and Th1/Th17 polarization (Figs. 10–11). Although rodent models of eating disorders have been invaluable for uncovering neurobehavioral mechanisms, immune-related data from these models remain limited. Only a few studies have examined T-cell function, cytokine production, or gut barrier integrity, and the findings are often inconsistent. Consequently, much of our understanding of how eating disorder pathology interacts with the immune system still derives from human investigations, including clinical immunophenotyping, peripheral cytokine profiling, and gut permeability assays in patients.

In the ABA model, the FRW group exhibited a suppressive effect on proliferating $CD4^+$ and $CD8^+$ T cells in both tissues, including Th1, Th2, and Treg subsets, along with decreased production of IFN-γ, TGF-β, and IL-17, indicating a profound impairment of adaptive immune homeostasis (Figs. 10, 12). These results indicate that the ABA model reproduces an immunosuppressive state driven by metabolic deficiency and excessive physical activity. These findings are consistent with clinical observations in patients with AN, in whom chronic malnutrition and hypercortisolemia are associated with lymphopenia, impaired T-cell responsiveness, and reduced cytokine production (39). In anorexic patients, similarly reduced concentrations of TGF-β have been reported (40), although these were measured in serum rather than by flow cytometry.

The reduced IFN-γ production observed in ABA mice aligns with previous reports describing decreased IFN-γ levels under malnutrition. Nutritional deficiency is known to suppress Th1-mediated immune responses, resulting in reduced production of pro-inflammatory cytokines such as IFN-γ (41–43).

Additionally, AN has been associated with alterations in the Th1/Th2 immune balance, with some studies suggesting a shift toward Th2-dominated or immunoregulatory responses. In line with this interpretation, we observed increased IL-10 production (Fig. 12), a key anti-inflammatory cytokine associated with regulatory and, in some contexts, Th2-related immune responses. This increase may also be related to the high physical activity characteristic of the ABA model, as IL-10 production has been reported to increase following physical exercise (44, 45). Importantly, however, IL-10 levels did not differ between patients with AN and healthy controls in a clinical study (46), suggesting that the increased IL-10 production observed in our ABA model may reflect the combined effects of food restriction and excessive physical activity rather than AN-like pathology alone.

Both stress stimuli in the BED model induced proliferative, Th1-skewed immune activation in both tested tissues, accompanied by compensatory expansion of regulatory T cells, suggesting simultaneous inflammatory activation and immune-regulatory counterbalance. Increased proliferation of $CD4^+$, $CD8^+$, and T-bet–expressing T cells in both food-restricted and restrained mice indicates stress-associated T-cell activation. The parallel expansion of proliferating regulatory T cells suggests induction of compensatory immune-regulatory mechanisms, consistent with controlled mucosal immune activation rather than overt inflammatory pathology. One of the most prominent findings was the increased

proliferative activity of both $CD4^+$ and $CD8^+$ T cells in the MLN and spleen. Enhanced Ki-67 expression suggests that food restriction and restraint stress promote T-cell activation and expansion, potentially reflecting heightened immune surveillance or responses to stress-induced physiological alterations (Fig. 11). Similar increases in T-cell proliferation have been reported in models of psychological stress and nutritional imbalance, where neuroendocrine mediators can directly influence lymphocyte activation and differentiation (47). The observation that these changes occurred in both intestinal and systemic lymphoid tissues suggests that BED-associated stressors exert widespread immunomodulatory effects rather than being restricted to the gut environment.

Despite increased Treg abundance, frequencies of $CD4^+TGF\text{-}\beta^+$ cells were significantly reduced in both experimental groups of BED mice. Because TGF-β is a key mediator of Treg suppressive function, these findings suggest that regulatory activity may be functionally impaired despite numerical expansion of Tregs (Fig. 11). This dissociation between Treg frequency and suppressive capacity has been described in several inflammatory conditions and may contribute to the persistence of low-grade inflammation (48, 49). The increased frequencies and proliferation of $CD4^+T\text{-}bet^+$ cells in both MLN and spleen indicate pronounced activation of Th1-associated immune responses (Fig. 11). This observation was further supported by increased frequencies of IFN-γ-producing $CD4^+$ T cells in the spleen. Th1 polarization is commonly associated with stress-induced immune activation and has been linked to the production of pro-inflammatory cytokines. In addition to Th1 responses, our data demonstrate enhanced Th17-associated immunity, particularly in food-restricted animals. Increased frequencies of IL-17A-producing $CD4^+$ T cells in both MLN and spleen suggest that short nutritional stress promotes differentiation or activation of Th17 cells (Fig. 13). Th17 responses play critical roles in mucosal immunity but can also contribute to chronic inflammation when dysregulated. The simultaneous increase in Th1- and Th17-associated responses observed in this study is notable since these populations often cooperate to amplify inflammatory processes and tissue damage. Previous studies have shown that stress-related neuroimmune signaling can promote both Th1 and Th17 polarization, supporting the interpretation that BED-associated conditions favor pro-inflammatory immune programming (50, 51). Together, these findings demonstrate that food restriction and restraint stress induce a complex pattern of immune dysregulation characterized by enhanced T-cell activation, expansion of Th1- and Th17-associated responses, altered T-cell subset distribution, and impaired regulatory cytokine production.

The coexistence of increased Treg frequencies with diminished TGF-β production suggests that compensatory regulatory mechanisms are activated but may be insufficient to control inflammation. We did not detect significant changes in IL-10 production by $CD4^+$ T cells in either the MLN or spleen of BED mice (Fig. 13). IL-10 is a key anti-inflammatory cytokine involved in maintaining immune tolerance and limiting excessive inflammatory responses (52). Increased frequencies of $CD8^+IL\text{-}10^+$ T cells were observed in both experimental groups; however, this population remained relatively scarce, suggesting that its overall contribution to immune regulation is likely limited (Fig. 13). Therefore, despite evidence of compensatory regulatory responses, such as increased Treg frequencies, IL-10-mediated immunoregulation does not appear to be substantially enhanced in this model. These findings differ from previous clinical observations describing reduced IL-10 levels in patients with BED (53). This

discrepancy may reflect important differences between human disease and experimental mouse models. Clinical studies measure systemic cytokine concentrations influenced by multiple immune and metabolic factors, whereas the present study specifically assessed intracellular cytokine production by defined T-cell subsets. Furthermore, the BED model reproduces selected behavioral and physiological aspects of the disorder but may not fully capture the chronic metabolic, endocrine, and psychological alterations present in patients with BED. Nevertheless, the lack of significant changes in $CD4^+IL\text{-}10^+$ T cells, together with reduced TGF-β-producing $CD4^+$ cells, suggests that impaired immune regulation in this model is driven primarily by defects in TGF-β-associated pathways rather than by diminished IL-10 production.

We are aware that food restriction increased the frequency of $CD4^+IL\text{-}17^+$ cells in the BED paradigm, whereas a similar effect was not observed in the ABA model. Although both paradigms involve reduced food intake, the broader experimental context differs substantially. In the ABA model, animals are exposed to prolonged caloric restriction combined with excessive physical activity, resulting in marked weight loss and a profound negative energy balance that may promote immunosuppressive mechanisms and limit Th17 responses. In contrast, food restriction in the BED model is shorter in duration and followed by refeeding, while animals are simultaneously exposed to behavioral stress associated with the binge-eating protocol. These differences may favor the development of a transient pro-inflammatory environment and increased Th17 polarization. Therefore, the immunological consequences of food restriction appear to be highly context-dependent and influenced by the duration of restriction, metabolic status, refeeding, and associated stressors.

A major strength of this study is the comprehensive characterization of gut barrier integrity and immune responses in two widely used mouse models of eating disorders. To our knowledge, this is the first study to combine functional assessment of intestinal permeability with analysis of TJ protein–related gene expression and detailed immunological profiling of T-cell responses and cytokine production in both mesenteric lymph nodes and spleen. These data provide new insight into the relationship between barrier dysfunction and immune alterations in ABA and BED models.

However, several limitations should be acknowledged. First, intestinal permeability was assessed using orally administered FITC-dextran, a widely used but relatively insensitive method that may not detect subtle changes in barrier function. Second, our analysis of barrier-associated proteins was limited to a selected panel of genes. Transcriptomic approaches, such as RNA sequencing, would allow a broader and less biased characterization of molecular pathways involved in barrier regulation and eating-disorder pathophysiology. Finally, flow-cytometric analysis was restricted to a limited number of cytokines and T-cell subsets. As a result, additional immune populations and signaling pathways potentially involved in disease-associated immune dysregulation may have remained undetected. Future studies using more comprehensive immune profiling approaches will be necessary to further elucidate the complex interactions between barrier function and immune responses.

Female mice were used in the ABA experiments, whereas male mice were used in the BED experiments. The selection of sex was based on established literature and optimization of each model. The ABA paradigm is most commonly conducted using female rodents because it reliably reproduces key behavioral and physiological features of AN, a disorder with a markedly higher prevalence in females. In contrast, the BED model employed in this study was previously validated in male mice and was therefore implemented using the same sex to ensure robustness and comparability with published findings. Moreover, in our model of BED, food restriction was implemented primarily as a stressor and environmental challenge rather than as a means of inducing compensatory feeding. Because different sexes were used in the ABA and BED models, direct comparisons between models should be interpreted as comparisons of disorder endotypes within their respective validated experimental paradigms rather than as assessments of sex-specific effects. The present study was not designed or powered to evaluate sex differences and the potential influence of sex on gut barrier function and immune responses, and this limitation should be noted. Nevertheless, we acknowledge that food restriction may also engage homeostatic mechanisms and therefore constitutes a limitation of the model.Taken together, the present findings show that the ABA and BED models produce opposing immune signatures. In both models, a notable observation was the strong impact of environmental or behavioral stressors on immune phenotype. In the ABA model, voluntary wheel running had a dominant suppressive effect on T cell proliferation, while restraint stress in the BED model enhanced cytotoxic and Th1-associated responses.

Conclusion

Our findings demonstrate distinct gut–immune alterations in mouse models of restrictive and binge-eating–related phenotypes. In the ABA model, food restriction combined with excessive physical activity increased intestinal permeability and was associated with an overall immunosuppressive phenotype. In contrast, the BED model showed marked alterations in barrier-related gene expression without measurable increases in intestinal permeability, together with enhanced T-cell proliferation and predominantly Th1/Th17-associated responses. These findings suggest that gut barrier and immune alterations are important but phenotype-specific components of eating disorder pathophysiology.

Abbreviations

ABA	activity-based anorexia
ACK	ammonium-chloride-potassium lysis buffer
ACTB	actin beta
BBB	blood-brain barrier
BED	binge-eating disorder

Cldn	claudin
CSP	conditioned suppression paradigm
Ctrl	control
ELISA	enzyme-linked immunosorbent assay
FITC	fluorescein isothiocyanate
FMO	fluorescence-minus-one
FR	food restriction
FRW	food restriction + wheel
GAPDH	glyceraldehyde 3-phosphate dehydrogenase
IFN-γ	interferon gamma
IL	interleukin
JAMs	junctional adhesion molecules
LBP	**lipopolysaccharide-binding protein**
M/F	male/female
MLN	mesenteric lymph nodes
Muc	mucin
Ocln	occludin
PCR	polymerase chain reaction
R	restraint
RT-qPCR	quantitative reverse transcription polymerase chain reaction
SAA	amyloid A
sCD14	**secretory CD14**
TGF-β	transforming growth factor beta
Th	T helper

TJ	tight junction
TJP	tight junction protein
Tregs	T regularory cells
W	wheel

Declarations

Funding

The study was supported by the Ministry of Health of the Czech Republic under grant nr. NU22-04-00010 and NU23-04-00381 and by the Ministry of Education, Youth, and Sports of the Czech Republic under grant Talking microbes - understanding microbial interactions within One Health framework (CZ.02.01.01/00/22_008/0004597).

Author contributions

Petra Prochazkova: Conceptualization, Funding acquisition, Resources, Data curation, Formal analysis, Investigation, Methodology, Validation, Visualization, Writing – original draft, Writing – review & editing.

Helena Knotkova: Investigation, Formal analysis.

Janet Luthar: Investigation, Formal analysis, Data curation.

Radka Roubalova: Methodology, Validation, Writing – review & editing.

Michal Kraus: Conceptualization, Investigation.

Toghrul Naghiyev: Investigation.

Enrico Patrono: Investigation.

Helena Tlaskalova-Hogenova: Supervision, Methodology.

Hana Papezova: Supervision, Resources, Project administration, Funding acquisition.

Declaration of interest statement

All authors declare that they have no financial or non-financial competing interests.

Data availability statement

The data generated and analyzed in this study are available in the Open Research Repository Zenodo under the following DOI: 10.5281/zenodo.20595839.

References

1. Foldi CJ. Taking better advantage of the activity-based anorexia model. Trends Mol Med. 2024;30(4):330–8.
2. Brown RM, James MH. Binge eating, overeating and food addiction: Approaches for examining food overconsumption in laboratory rodents. Prog Neuropsychopharmacol Biol Psychiatry. 2023;123:110717.
3. Patrono E, Di Segni M, Patella L, Andolina D, Valzania A, Latagliata EC, et al. When chocolate seeking becomes compulsion: gene-environment interplay. PLoS ONE. 2015;10(3):e0120191.
4. Vajdova D, Jezkova J, Prochazkova P, Roubalova R, Patrono E. Evidence for food-related and non-food-related maladaptive preference in a mouse model of binge eating disorder. Front Behav Neurosci. 2025;19:1653807.
5. Scharner S, Stengel A. Animal Models for Anorexia Nervosa-A Systematic Review. Front Hum Neurosci. 2020;14:596381.
6. Rehn S, Raymond JS, Boakes RA, Kendig MD, Leenaars CHC. Behavioural and physiological effects of binge eating: A systematic review and meta-analysis of animal models. Neurosci Biobehav Rev. 2025;173:106135.
7. Rehn S, Raymond JS, Boakes RA, Leenaars CHC. A systematic review and meta-analysis of animal models of binge eating - Part 1: Definitions and food/drink intake outcomes. Neurosci Biobehav Rev. 2022;132:1137–56.
8. Gunzel D, Yu AS. Claudins and the modulation of tight junction permeability. Physiol Rev. 2013;93(2):525–69.
9. Zihni C, Mills C, Matter K, Balda MS. Tight junctions: from simple barriers to multifunctional molecular gates. Nat Rev Mol Cell Biol. 2016;17(9):564–80.
10. Cani PD, Osto M, Geurts L, Everard A. Involvement of gut microbiota in the development of low-grade inflammation and type 2 diabetes associated with obesity. Gut Microbes. 2012;3(4):279–88.
11. Marchi N, Granata T, Ghosh C, Janigro D. Blood-brain barrier dysfunction and epilepsy: pathophysiologic role and therapeutic approaches. Epilepsia. 2012;53(11):1877–86.
12. Butler MJ, Perrini AA, Eckel LA. The Role of the Gut Microbiome, Immunity, and Neuroinflammation in the Pathophysiology of Eating Disorders. Nutrients. 2021;13(2).
13. Lochhead JJ, Yang J, Ronaldson PT, Davis TP. Structure, Function, and Regulation of the Blood-Brain Barrier Tight Junction in Central Nervous System Disorders. Front Physiol. 2020;11:914.
14. Woting A, Blaut M. Small Intestinal Permeability and Gut-Transit Time Determined with Low and High Molecular Weight Fluorescein Isothiocyanate-Dextrans in C3H Mice. Nutrients. 2018;10(6).

15. Olfe J, Domanska G, Schuett C, Kiank C. Different stress-related phenotypes of BALB/c mice from in-house or vendor: alterations of the sympathetic and HPA axis responsiveness. BMC Physiol. 2010;10:2.
16. Young JK. Anorexia nervosa and estrogen: current status of the hypothesis. Neurosci Biobehav Rev. 2010;34(8):1195–200.
17. Casimiro I, Stull ND, Tersey SA, Mirmira RG. Phenotypic sexual dimorphism in response to dietary fat manipulation in C57BL/6J mice. J Diabetes Complications. 2021;35(2):107795.
18. Berger G, Corris JD, Fields SE, Hao L, Scarpa LL, Bello NT. Systematic Review of Binge Eating Rodent Models for Developing Novel or Repurposing Existing Pharmacotherapies. Biomolecules. 2023;13(5).
19. Xie F, Xiao P, Chen D, Xu L, Zhang B. miRDeepFinder: a miRNA analysis tool for deep sequencing of plant small RNAs. Plant Mol Biol. 2012.
20. American Psychiatric Association A. Diagnostic and Statistical Manual of Mental Disorders. Dsm-5. 5th ed. Washington, D.C, USA: American Psychiatric Publishing; 2013.
21. Turner JR. Intestinal mucosal barrier function in health and disease. Nat Rev Immunol. 2009;9(11):799–809.
22. Yan Y, Kolachala V, Dalmasso G, Nguyen H, Laroui H, Sitaraman SV, et al. Temporal and spatial analysis of clinical and molecular parameters in dextran sodium sulfate induced colitis. PLoS ONE. 2009;4(6):e6073.
23. Jesus P, Ouelaa W, Francois M, Riachy L, Guerin C, Aziz M, et al. Alteration of intestinal barrier function during activity-based anorexia in mice. Clin Nutr. 2014;33(6):1046–53.
24. Ribeiro TA, Breznik JA, Kennedy KM, Yeo E, Kennelly BKE, Jazwiec PA, et al. Intestinal permeability and peripheral immune cell composition are altered by pregnancy and adiposity at mid- and late-gestation in the mouse. PLoS ONE. 2023;18(8):e0284972.
25. Natarajan R, Northrop N, Yamamoto B. Fluorescein Isothiocyanate (FITC)-Dextran Extravasation as a Measure of Blood-Brain Barrier Permeability. Curr Protoc Neurosci. 2017;79:9. 58 1–9 15.
26. Scalise AA, Kakogiannos N, Zanardi F, Iannelli F, Giannotta M. The blood-brain and gut-vascular barriers: from the perspective of claudins. Tissue Barriers. 2021;9(3):1926190.
27. Voges L, Weiss F, Branco AT, Fromm M, Krug SM. Expression and Localization Profiles of Tight Junction Proteins in Immune Cells Depend on Their Activation Status. Int J Mol Sci. 2024;25(9).
28. Lu Z, Ding L, Lu Q, Chen YH. Claudins in intestines: Distribution and functional significance in health and diseases. Tissue Barriers. 2013;1(3):e24978.
29. Kalucka J, de Rooij L, Goveia J, Rohlenova K, Dumas SJ, Meta E, et al. Single-Cell Transcriptome Atlas of Murine Endothelial Cells. Cell. 2020;180(4):764–79. e20.
30. Holmes JL, Van Itallie CM, Rasmussen JE, Anderson JM. Claudin profiling in the mouse during postnatal intestinal development and along the gastrointestinal tract reveals complex expression patterns. Gene Expr Patterns. 2006;6(6):581–8.

31. Roubalova R, Prochazkova P, Kovarova T, Jezkova J, Hrncir T, Tlaskalova-Hogenova H, et al. Influence of the gut microbiome on appetite-regulating neuropeptides in the hypothalamus: Insight from conventional, antibiotic-treated, and germ-free mouse models of anorexia nervosa. Neurobiol Dis. 2024;193:106460.
32. Zeisel MB, Dhawan P, Baumert TF. Tight junction proteins in gastrointestinal and liver disease. Gut. 2019;68(3):547–61.
33. Luthar J, Patrono E, Prochazkova P, Kubisova G, Knotkova H, Vajdova D et al. Microbiome-Associated Changes in Feeding Behaviour in a Mouse Model of Binge Eating under review. 2026.
34. Nitta T, Hata M, Gotoh S, Seo Y, Sasaki H, Hashimoto N, et al. Size-selective loosening of the blood-brain barrier in claudin-5-deficient mice. J Cell Biol. 2003;161(3):653–60.
35. Shive CL, Jiang W, Anthony DD, Lederman MM. Soluble CD14 is a nonspecific marker of monocyte activation. AIDS. 2015;29(10):1263–5.
36. Kalla R, Kennedy NA, Ventham NT, Boyapati RK, Adams AT, Nimmo ER, et al. Serum Calprotectin: A Novel Diagnostic and Prognostic Marker in Inflammatory Bowel Diseases. Am J Gastroenterol. 2016;111(12):1796–805.
37. Sack GH. Jr. Serum amyloid A - a review. Mol Med. 2018;24(1):46.
38. Schumann RR, Leong SR, Flaggs GW, Gray PW, Wright SD, Mathison JC, et al. Structure and function of lipopolysaccharide binding protein. Science. 1990;249(4975):1429–31.
39. Sabel AL, Gaudiani JL, Statland B, Mehler PS. Hematological abnormalities in severe anorexia nervosa. Ann Hematol. 2013;92(5):605–13.
40. Corcos M, Guilbaud O, Chaouat G, Cayol V, Speranza M, Chambry J, et al. Cytokines and anorexia nervosa. Psychosom Med. 2001;63(3):502–4.
41. Gonzalez-Martinez H, Rodriguez L, Najera O, Cruz D, Miliar A, Dominguez A, et al. Expression of cytokine mRNA in lymphocytes of malnourished children. J Clin Immunol. 2008;28(5):593–9.
42. Gonzalez-Torres C, Gonzalez-Martinez H, Miliar A, Najera O, Graniel J, Firo V, et al. Effect of malnutrition on the expression of cytokines involved in Th1 cell differentiation. Nutrients. 2013;5(2):579–93.
43. Rodriguez L, Gonzalez C, Flores L, Jimenez-Zamudio L, Graniel J, Ortiz R. Assessment by flow cytometry of cytokine production in malnourished children. Clin Diagn Lab Immunol. 2005;12(4):502–7.
44. Helmark IC, Mikkelsen UR, Borglum J, Rothe A, Petersen MC, Andersen O, et al. Exercise increases interleukin-10 levels both intraarticularly and peri-synovially in patients with knee osteoarthritis: a randomized controlled trial. Arthritis Res Ther. 2010;12(4):R126.
45. Ribeiro F, Alves AJ, Teixeira M, Miranda F, Azevedo C, Duarte JA, et al. Exercise training increases interleukin-10 after an acute myocardial infarction: a randomised clinical trial. Int J Sports Med. 2012;33(3):192–8.

46. Dalton B, Campbell IC, Chung R, Breen G, Schmidt U, Himmerich H. Inflammatory Markers in Anorexia Nervosa: An Exploratory Study. Nutrients. 2018;10(11).
47. Lehman H, Ballow MC, editors. Nutritional and stress effects on immunologic function2020.
48. Sojka DK, Huang YH, Fowell DJ. Mechanisms of regulatory T-cell suppression - a diverse arsenal for a moving target. Immunology. 2008;124(1):13–22.
49. Yang H, Zhang H, Xia N, Cheng X. Regulatory T cells in cancer and inflammation. Signal Transduct Target Ther. 2026;11(1).
50. Shimba A, Cui G, Abe S, Hirota K, Miyauchi E, Takami D, et al. Stress-induced glucocorticoids enhance acute inflammation by promoting the differentiation of Th17 cells. Cell Rep. 2025;44(8):116093.
51. Zhao J, Liu J, Denney J, Li C, Li F, Chang F, et al. TLR2 Involved in Naive CD4 + T Cells Rescues Stress-Induced Immune Suppression by Regulating Th1/Th2 and Th17. Neuroimmunomodulation. 2015;22(5):328–36.
52. Opal SM, DePalo VA. Anti-inflammatory cytokines. Chest. 2000;117(4):1162–72.
53. Caroleo M, Carbone EA, Greco M, Corigliano DM, Arcidiacono B, Fazia G et al. Brain-Behavior-Immune Interaction: Serum Cytokines and Growth Factors in Patients with Eating Disorders at Extremes of the Body Mass Index (BMI) Spectrum. Nutrients. 2019;11(9).

Table 1

Table 1 is available in the Supplementary Files section.

Figures

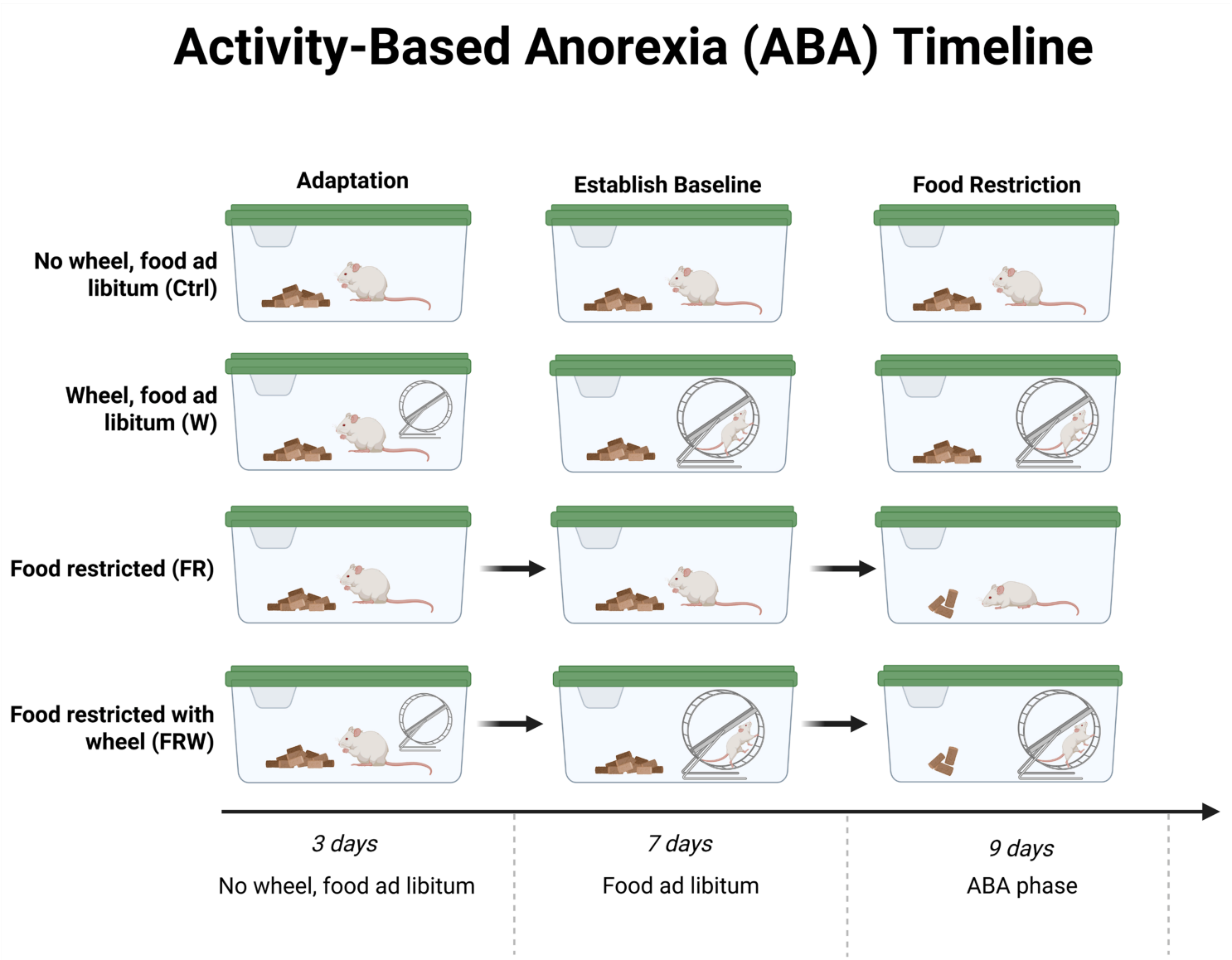


Figure 1

Timeline of activity-based anorexia (ABA) model (female Balb/c).. Schematic representation of the experimental timeline showing the acclimatization phase, establishment of baseline activity and food intake, and subsequent food-restriction phase. Mice were divided into four experimental groups, including two groups with access to running wheels and two groups without wheel access, with food restriction applied as indicated. Created with Biorender.

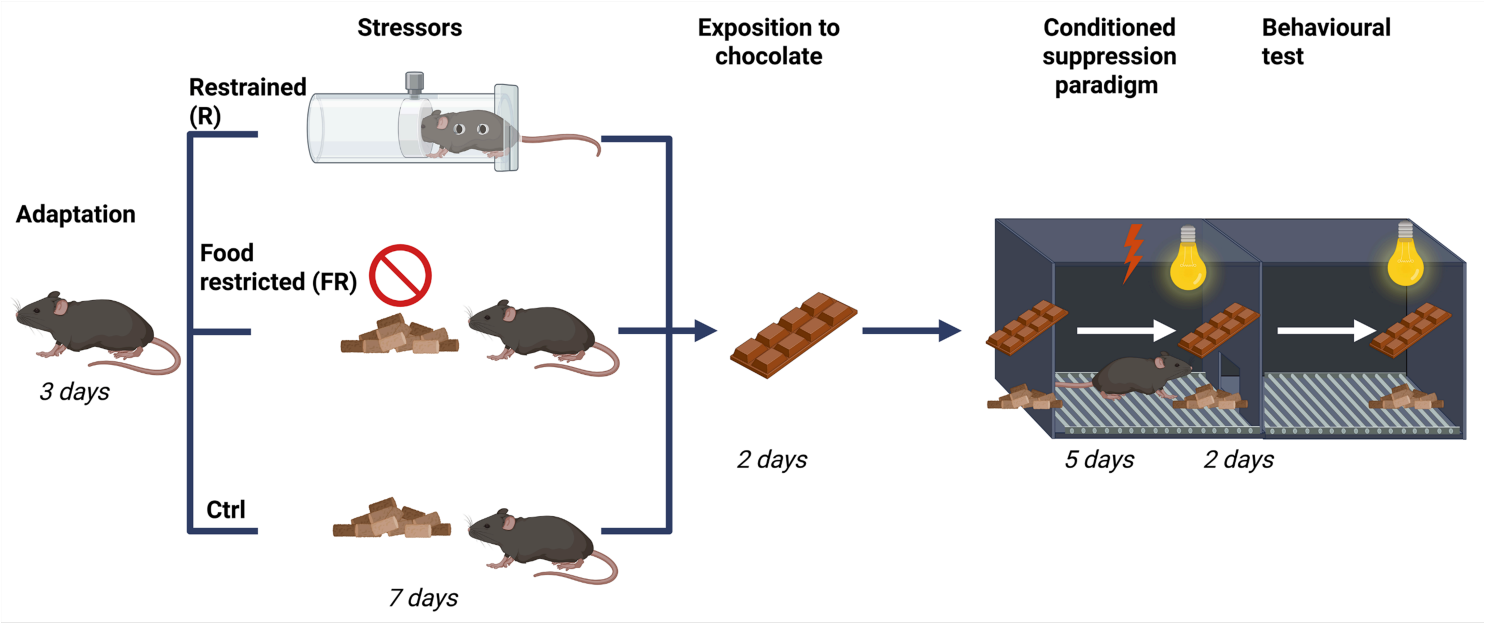


Figure 2

Timeline of binge-eating anorexia (BED) model (male C57Bl/6). Schematic representation of the experimental design, including the adaptation phase, exposure to the experimental stressors (food restriction and restraint stress), repeated access to chocolate, conditioned suppression paradigm, and subsequent behavioral testing. Mice were exposed to different combinations of stressors and food-related stimuli to induce binge-like eating behavior. The conditioned suppression paradigm was used to assess compulsive-like chocolate seeking. In this paradigm, mice were exposed to an aversive stimulus previously associated with a negative experience, creating a conflict between avoidance of the aversive context and motivation to obtain the palatable food. Continued chocolate seeking despite the aversive conditioning was interpreted as reduced behavioral suppression and compulsive-like food-seeking behavior. Created with Biorender.

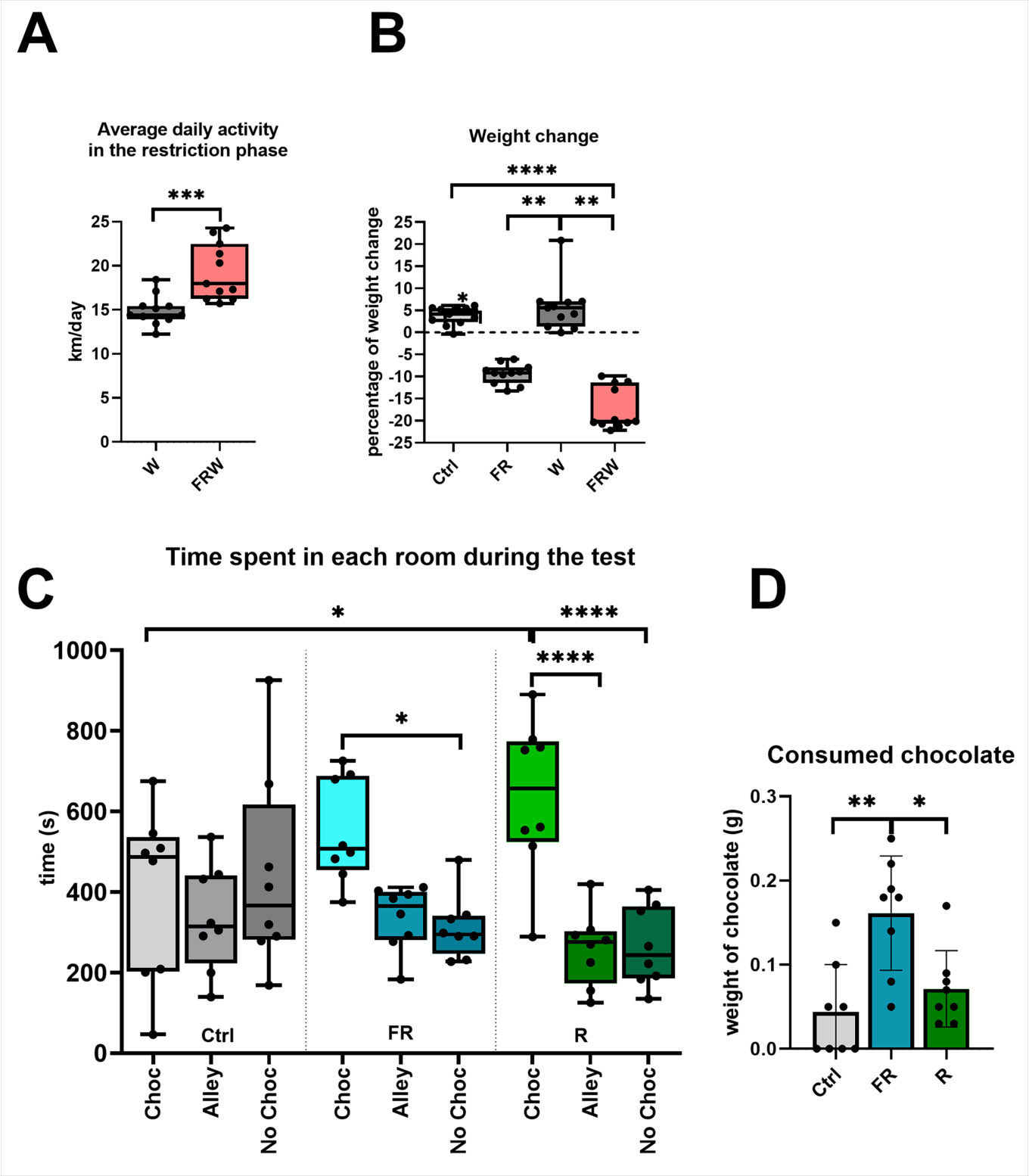


Figure 3

Establishment of core features of ABA and BED mouse models. (A) Average daily running activity during the restriction phase in the ABA model (female Balb/c), expressed as distance traveled (km/day); (B) Body-weight change in ABA mice throughout the restriction period, expressed as percentage change from baseline; (C) Time spent in each compartment of the apparatus in the BED model (male C57Bl/6) during behavioral assessment (Choc, Alley, No Choc); (D) Total amount of chocolate consumed by BED mice

*during the test session, expressed in grams. Values represent the mean ± SD or span the complete range with the mean ± SD, from minimum to maximum. Sample sizes: ABA = 11 mice/group; BED = 8 mice/group. Data from the ABA model were analyzed using the unpaired t-test or Kruskal-Wallis test with Dunn's post-test. Data from the BED model were analyzed using one-way ANOVA with Sidak's post hoc test. Asterisks indicate statistical significance: *p < 0.05; **p < 0.01; ***p < 0.001; ****p < 0.0001. Ctrl – control; Choc – chocolate; FR – food restriction; R – restraint; W – running wheel; FRW – food restriction with running wheel.*

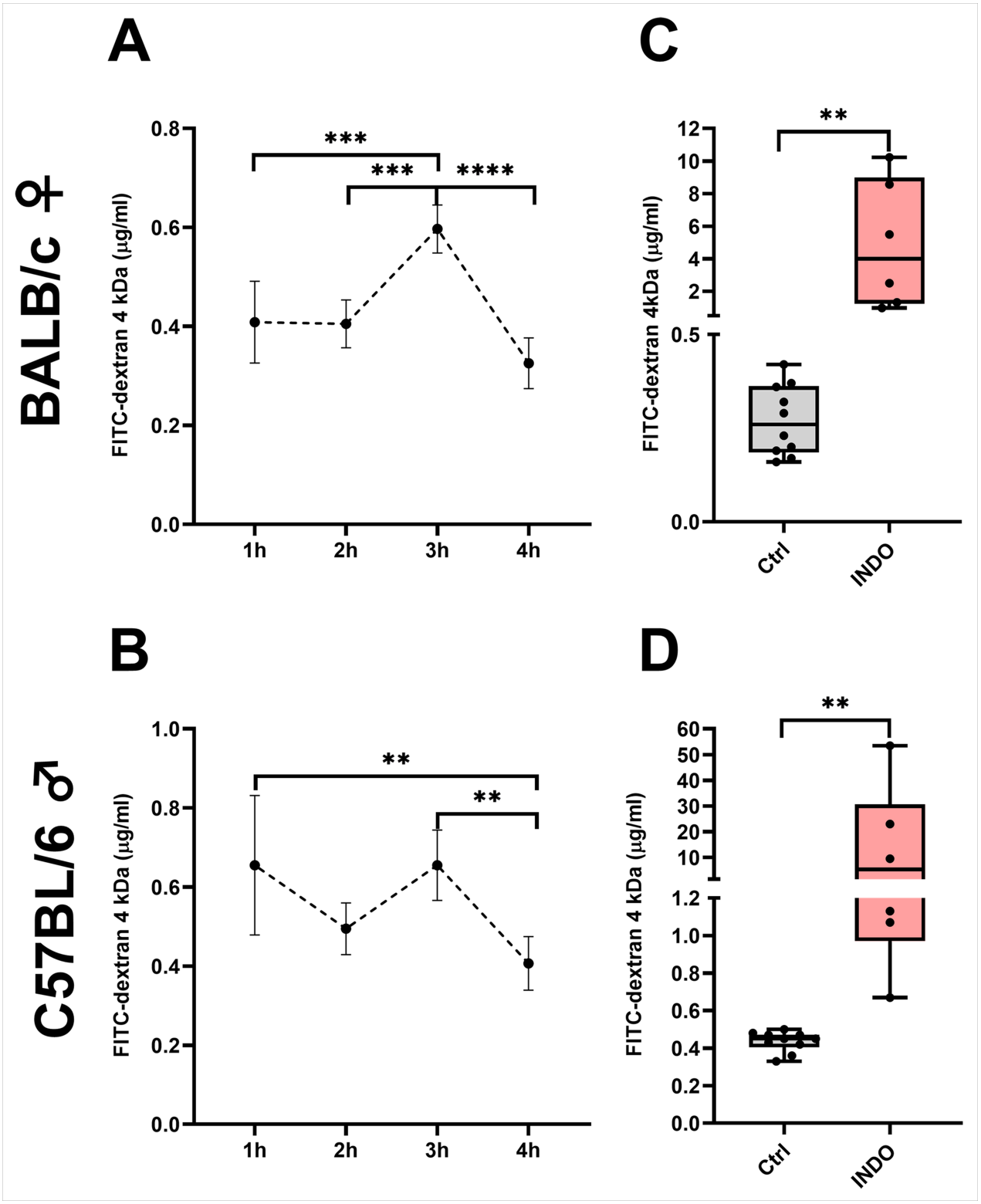


Figure 4

*Preliminary assessment of intestinal permeability in female BALB/c and male C57Bl/6 mice. Gut permeability was evaluated using oral gavage of 4 kDa FITC-dextran. Serum fluorescence was measured in serum at 1, 2, 3, and 4 hours post-gavage. Indomethacin-treated mice served as positive controls for increased gut permeability. Data are shown for BALB/c and C57BL/6 strains, indicating the amount of FITC-dextran translocated into circulation. (A, B) Time-dependent FITC-dextran translocation in BALB/c and C57BL/6 mice, respectively; (C, D) Serum FITC-dextran levels in control and indomethacin-treated BALB/c and C57BL/6 mice, respectively. Data were analyzed using one-way ANOVA with Tukey's post hoc test. Values represent the mean ± SD or span the complete range from minimum to maximum. Sample sizes: assessment of optimal blood collection time: BALB/c = 5, C57BL/6 = 6; indomethacin treatment: control = 10, indomethacin-treated = 6. Asterisks indicate statistical significance: **p < 0.01; ***p < 0.001; ****p < 0.0001. Ctrl – control; INDO – indomethacin.*

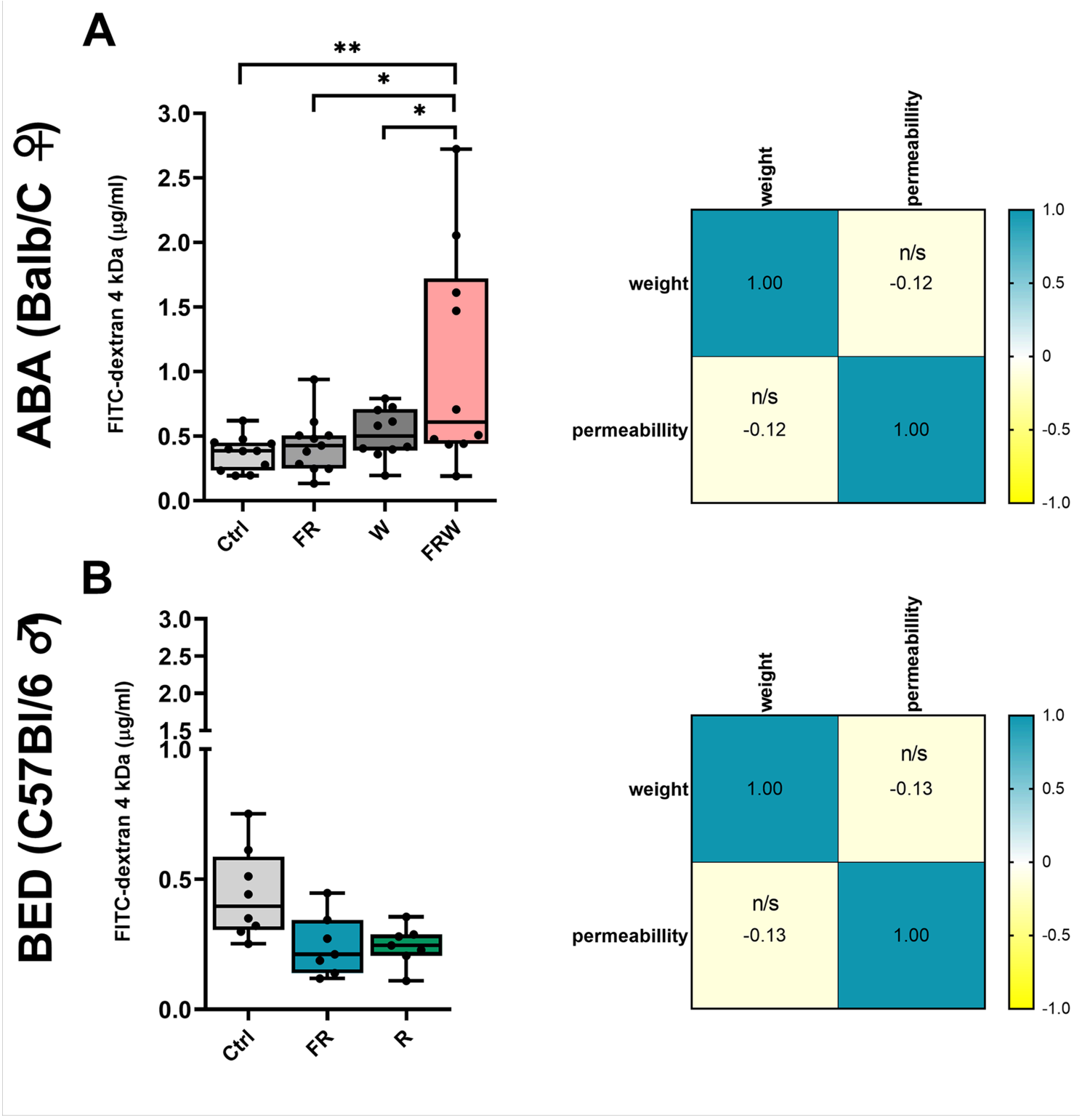


Figure 5

Gut permeability in ABA and BED mouse models. Gut permeability was evaluated using oral gavage of 4 kDa FITC-dextran. Data are shown for the ABA model (female BALB/c mice) and the BED model (male C57Bl/6), indicating intestinal permeability measured as serum FITC-dextran levels. (A) Serum FITC-dextran levels and Spearman correlation coefficients between body weight and intestinal permeability in the ABA model, (B) Serum FITC-dextran levels and Spearman correlation coefficients between body weight and

*intestinal permeability in the BED model. Data were analyzed using one-way ANOVA with Tukey's multiple-comparison test. Values show the complete range, from the minimum to the maximum. Sample sizes: ABA = 11 mice/group, BED = 8 mice/group. Asterisks denote statistical significance: n/s – non-significant; *p < 0.05; **p < 0.01. Ctrl – control; R – restraint; W – running wheel; FRW – food restriction with running wheel.*

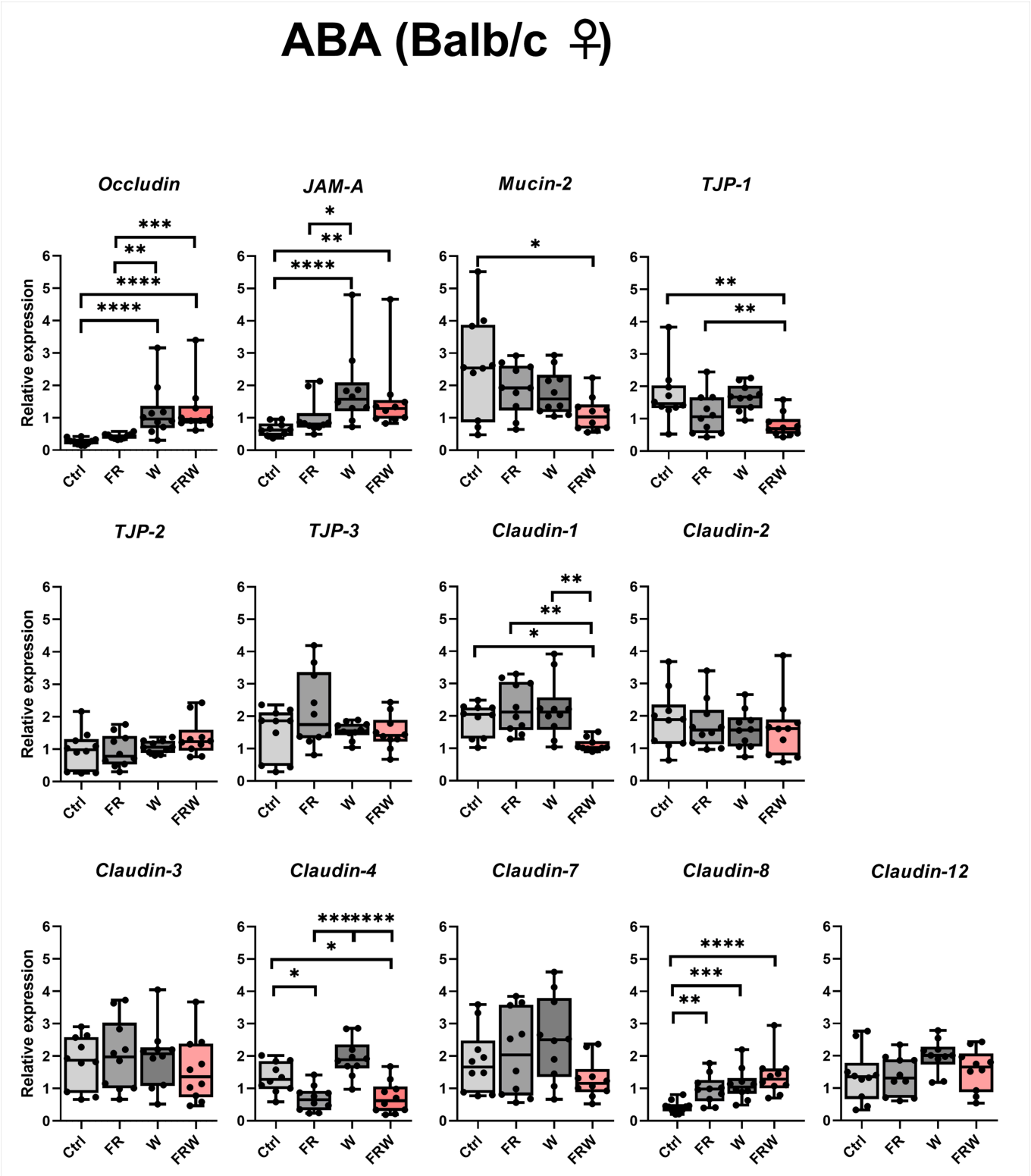


Figure 6

*mRNA expression of intestinal barrier-associated genes in the colon of ABA mice (female Balb/c). Relative mRNA transcript levels were determined by qRT-PCR and normalized to Actb and Gapdh reference genes. Panel titles use protein names for readability; data represent expression of the corresponding genes. Values represent the complete range from minimum to maximum. Transformed data (λ = 0.1) were analyzed using one-way ANOVA with Tukey's post hoc test. Asterisks indicate statistical significance: *p < 0.05;, **p < 0.01; ***p < 0.001; ****p < 0.0001. Sample sizes: n = 10 mice/group. Ctrl – control; FR – food restriction; W – running wheel; FRW – food restriction with running wheel; JAM-A – junctional adhesion molecule A; TJP – tight-junction protein.*

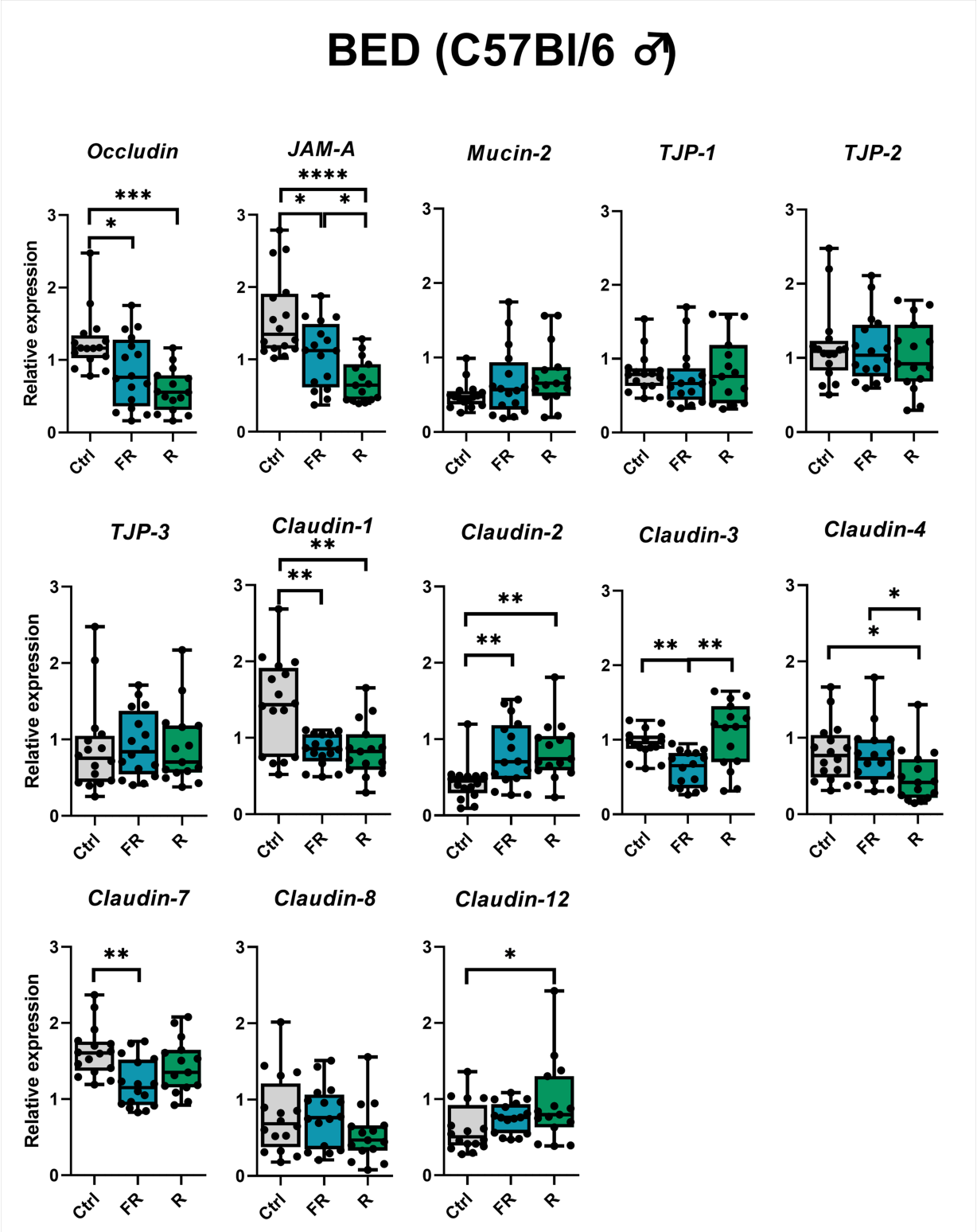


Figure 7

*mRNA expression of intestinal barrier–associated genes in the colon of BED mice (male C57Bl/6). Relative mRNA transcriptlevels were determined by qRT-PCR and normalized to Actb and Gapdh reference genes. Panel titles use protein names for readability; data represent expression of the corresponding genes. Values represent the full range from minimum to maximum. Transformed data (λ = 0.1) were analyzed using one-way ANOVA with Tukey's post hoc test. Asterisks indicate statistical significance: *p < 0.05; **p < 0.01, ***p*

< 0.001. Sample sizes: n = 16 mice/group. Ctrl – control; FR – food restriction; R – restraint; JAM-A – junctional adhesion molecule A; TJP – tight-junction protein.

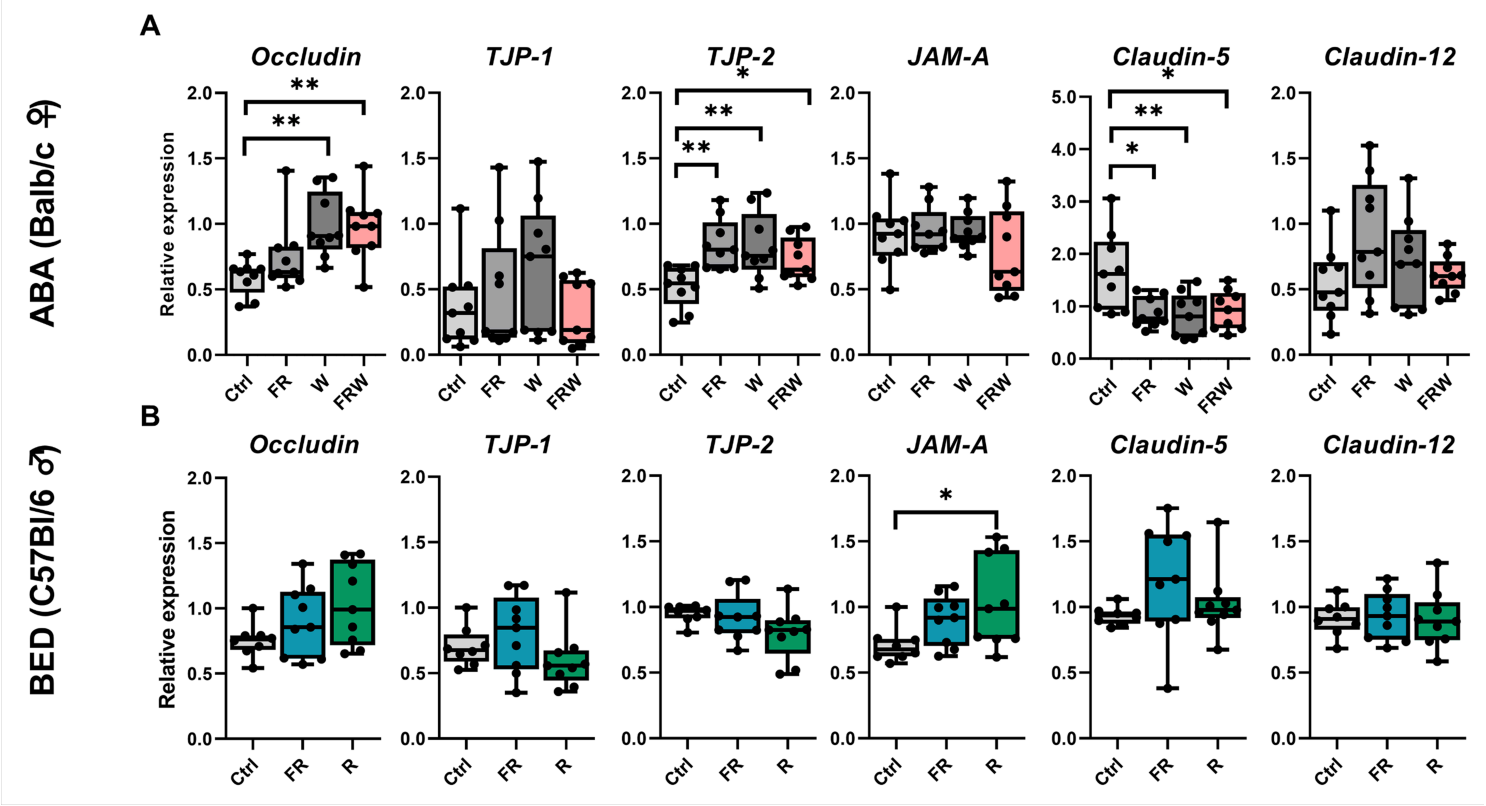


Figure 8

*mRNA expression of hypothalamic barrier–associated genes in (A) ABA (female Balb/c) and (B) BED (male C57Bl/6) mice. Relative mRNA transcript levels were determined by qRT-PCR and normalized to Actb and Gapdh reference genes. Panel titles use protein names for readability; data represent expression of the corresponding genes. Values represent the full range from minimum to maximum. Transformed data (λ = 0.1) were analyzed using one-way ANOVA with Tukey's post hoc test. Asterisks indicate statistical significance: n/s – non-significant; *p < 0.05; **p < 0.01. Sample sizes: n = 8 or 9 mice/group. Ctrl – control; FR – food restriction; W – running wheel; FRW – food restriction with running wheel; R – restraint; JAM-A – junctional adhesion molecule A; TJP – tight-junction protein.*

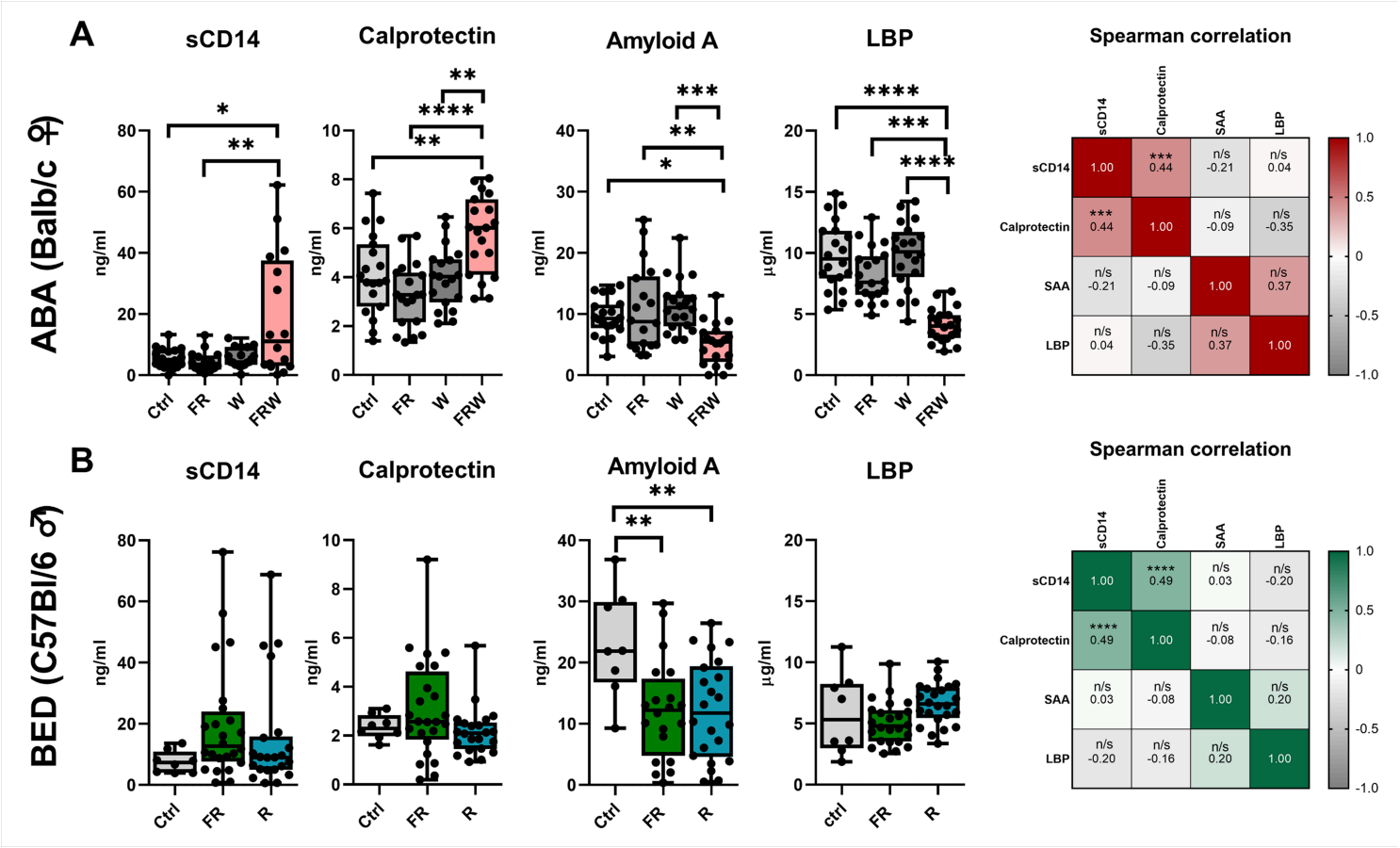


Figure 9

Serum concentrations of inflammatory and intestinal barrier-associated markers in (A) ABA (female Balb/c) and (B) BED (male C57Bl/6) model mice and their Spearman correlation. Red or green indicates a positive correlation; grey indicates a negative correlation. Data were transformed using the Box–Cox *transformation (λ = 0.1) and analyzed by one-way ANOVA with Tukey's post hoc test. Asterisks indicate statistical significance: *p < 0.05; **p < 0.01; ***p < 0.001; ****p < 0.0001. Values represent the full range from minimum to maximum. Sample size: ABA, n = 20 mice/group, BED, n = 24 mice/ group for FR and R, and n = 8 mice/group for controls. Ctrl – control; FR – food restriction; W – running wheel; FRW – food restriction with running wheel; LBP – lipopolysaccharide-binding protein; SAA – serum amyloid A; sCD14 – soluble CD14.*

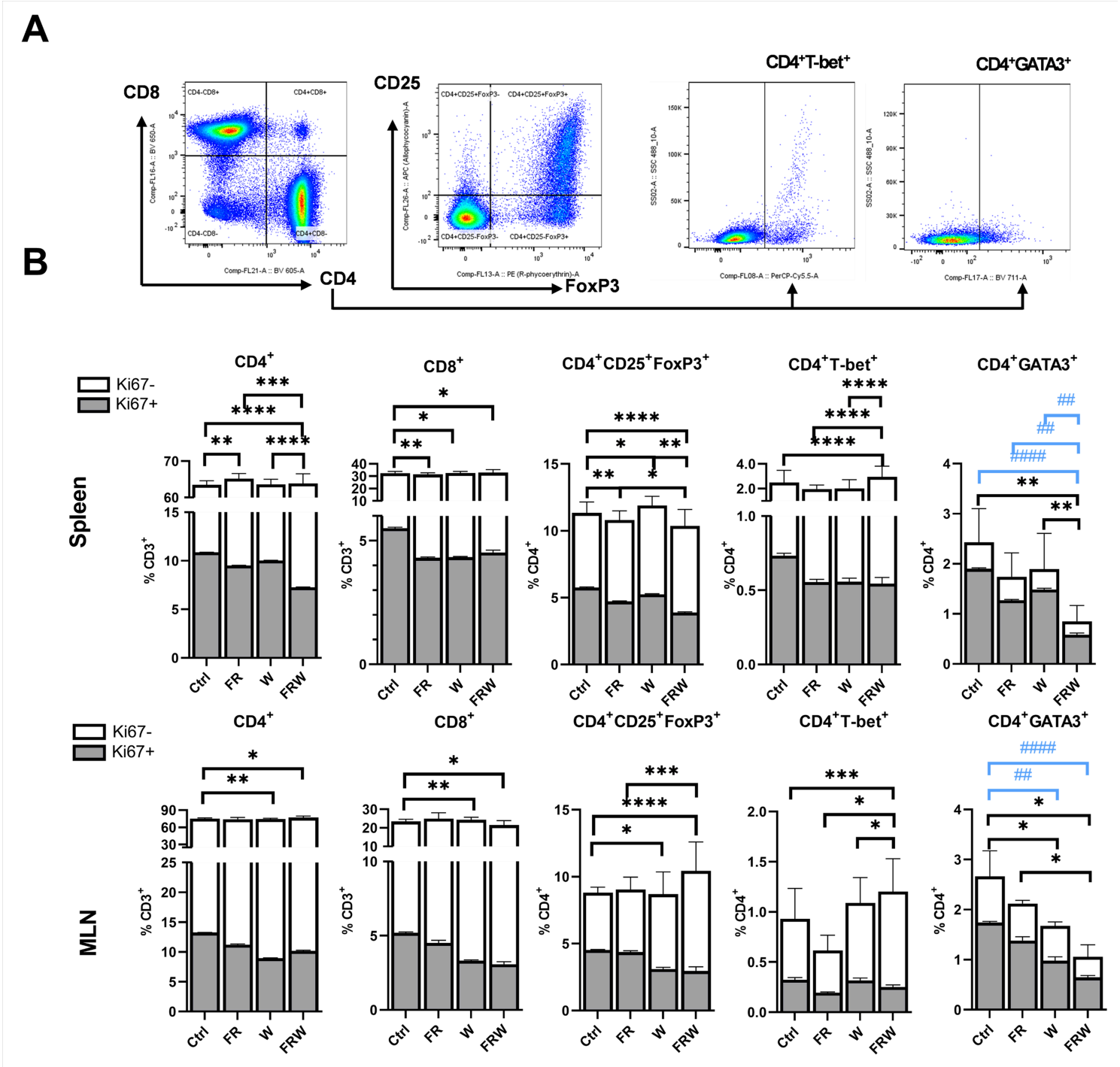


Figure 10

T-cell population in the spleen and mesenteric lymph nodes and s of ABA mice ***(female Balb/c)****. (A)* ***Representative flow cytometry gating strategy for T-cell subsets, (B)*** *T-cell composition and proliferation. Data were analyzed using one-way ANOVA with Tukey's post hoc test. Statistically significant differences in proliferating cell frequencies (Ki67$^+$ cells) are indicated by black brackets with asterisks, while statistically significant differences in total subset frequencies (Ki67$^+$ and Ki67$^-$ cells) between groups within the same T-cell subset are indicated by blue brackets with hash (#) symbols. $p < 0.05$; $p < 0.01$; $p < 0.001$; ****$p < 0.0001$; #$p < 0.05$; ##$p < 0.01$; ###$p < 0.001$; ####$p < 0.0001$. Values represent the mean ± SD. Sample sizes: n = 10*

mice/group. Ctrl – control; FR – food restriction; W – running wheel; FRW – food restriction with running wheel; MLN – mesenteric lymph nodes.

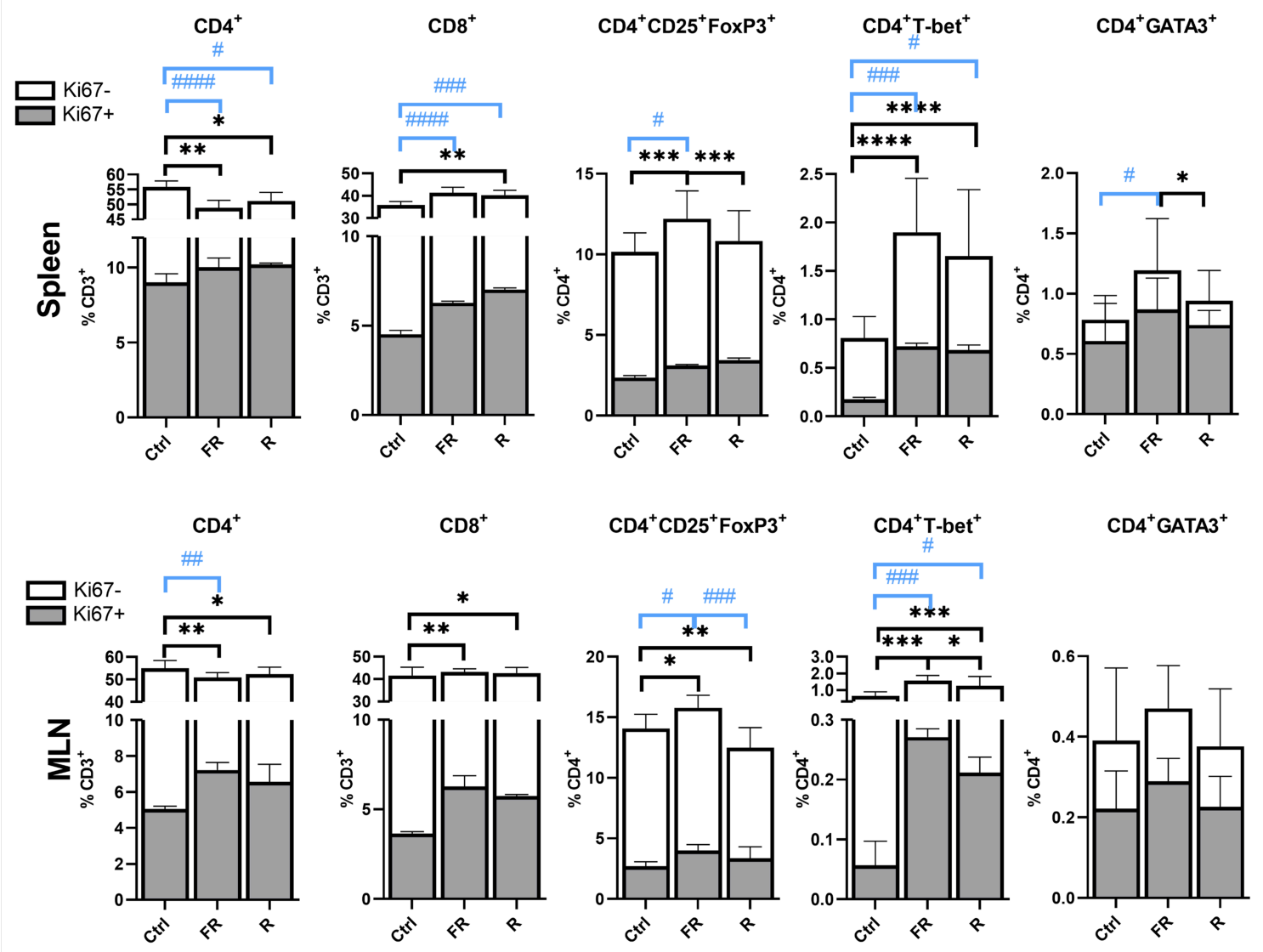


Figure 11

*T-cell subsets in the spleen and mesenteric lymph nodes of BED mice **(male C57Bl/6)**. Data were analyzed using one-way ANOVA with Tukey's post hoc test. Statistically significant differences in proliferating cell frequencies (Ki67$^+$ cells) are indicated by black brackets with asterisks, while statistically significant differences in total subset frequencies (Ki67$^+$ and Ki67$^-$ cells) between groups within the same T-cell subset are indicated by blue brackets with hash (#) symbols. * p < 0.05; **p < 0.01; ***p < 0.001; ****p < 0.0001, #p < 0.05; ##p < 0.01; ###p < 0.001; ####p < 0.0001. Values are shown as the mean ± SD. Sample sizes: n = 10 mice/group. Ctrl – control; FR – food restriction; W – running wheel; FRW – food restriction with running wheel; MLN – mesenteric lymph nodes.*

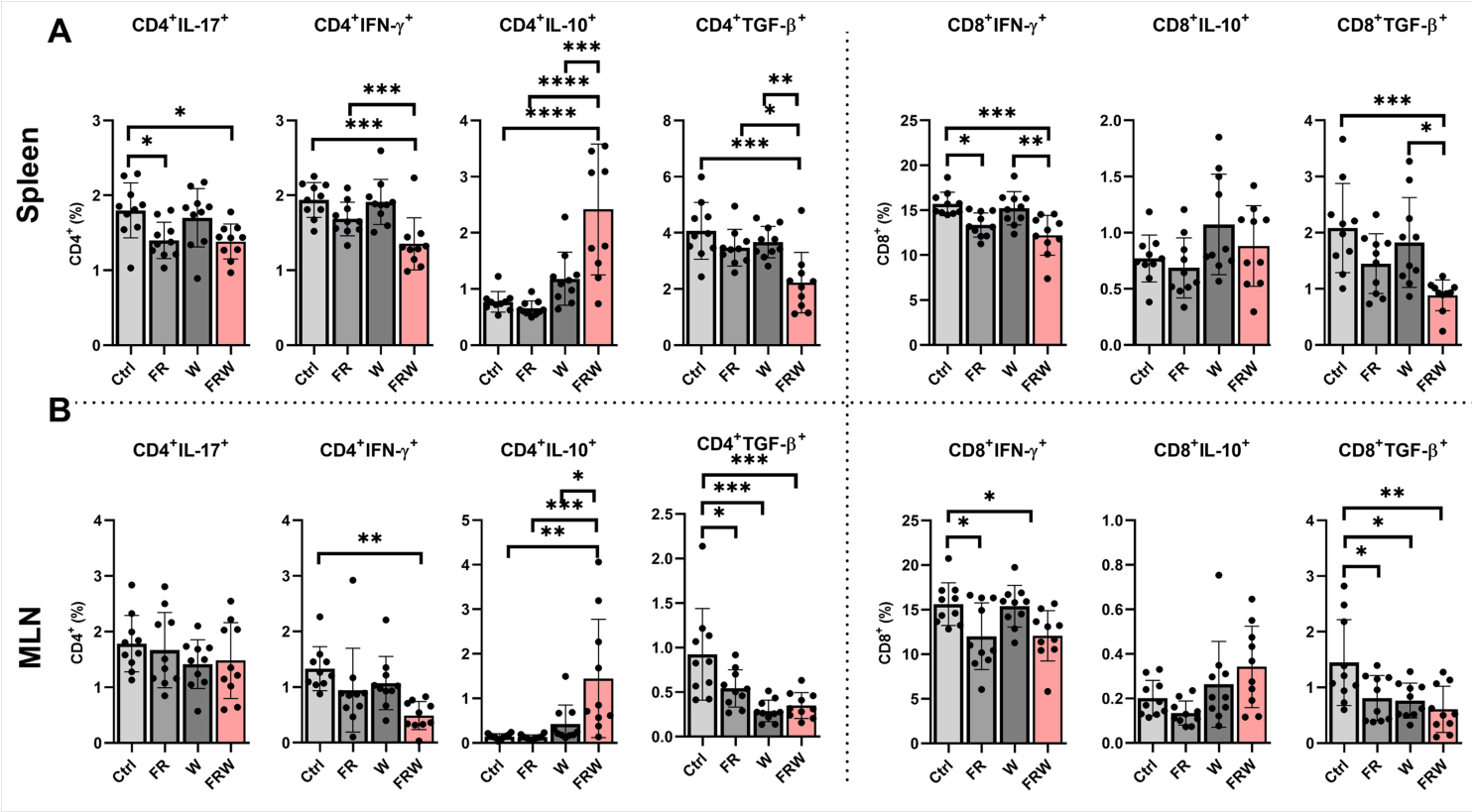


Figure 12

*Cytokine production in the spleen and mesenteric lymph nodes of ABA mice **(female Balb/c)**. (A) Cytokine production by CD4+ and CD8+ T cells in the spleen, (B) cytokine production by CD4+ and CD8+ T cells in MLN. Data were analyzed using one-way ANOVA with Tukey's post hoc test. Asterisks indicate statistical significance: *p < 0.05; **p < 0.01; ***p < 0.001; ****p < 0.0001. Values are shown as mean ± SD. Sample size: n = 10 mice/group. Ctrl – control; FR – food restriction; W – running wheel; FRW – food restriction with running wheel; MLN – mesenteric lymph nodes.*

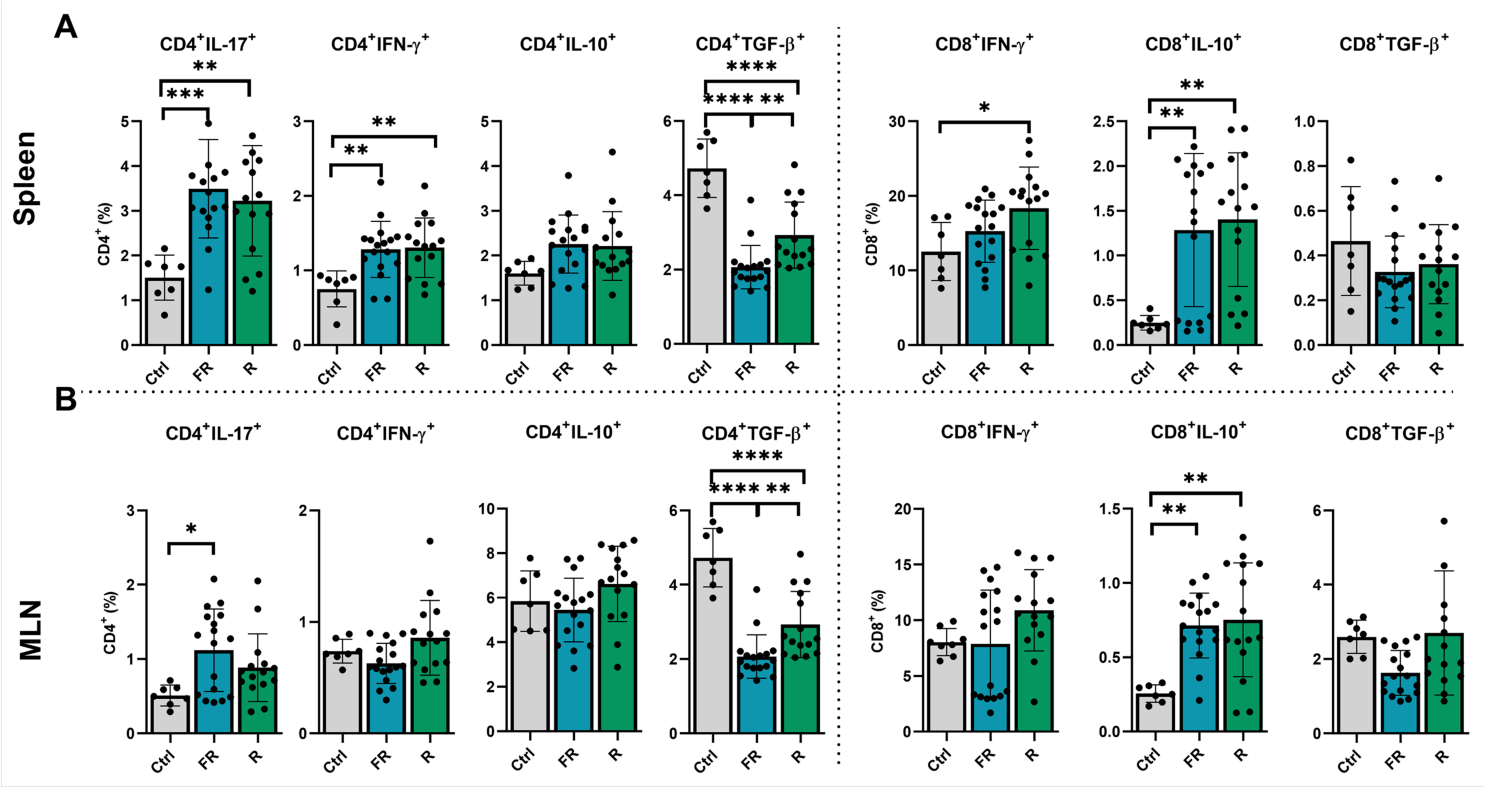


Figure 13

Cytokine production in the spleen and mesenteric lymph nodes of BED mice ***(male C57Bl/6)****. (A) Cytokine production by CD4+ and CD8+ T cells in the spleen, (B) cytokine production by CD4 and CD8 T cells in MLN. Data were analyzed using one-way ANOVA with Tukey's post hoc test. Asterisks indicate statistical significance: *p < 0.05; **p < 0.01;, ***p < 0.001; ****p < 0.0001. Values are shown as mean ± SD. Sample sizes: n = 8 mice/ctrl group, n = 16 mice/FR/R groups. Ctrl – control; FR – food restriction; R – restraint; MLN – mesenteric lymph nodes.*

Supplementary Files

This is a list of supplementary files associated with this preprint. Click to download.

- ProchazkovaSupplementarydata.docx
- Table1.docx